HIGH-RESOLUTION HYBRID PRIMITIVE-CONSERVATIVE UPWIND SCHEMES FOR THE DRIFT FLUX MODEL

KJELL KÅRE FJELDE[a] AND KENNETH HVISTENDAHL KARLSEN[b,a]

ABSTRACT. We consider a drift flux model describing one-dimensional isothermal gas-liquid flow in a long pipeline. The model consists of equations for the conservation of mass for each of the phases and the conservation of momentum of the mixture. In addition, an equation — the so-called gas slip relation — is supplied which relates the velocities of the two phases at any point. We present and demonstrate high-resolution hybrid primitive-conservative upwind schemes, which utilise a simple non-conservative MUSCL scheme in shock free flow regions and high-resolution conservative upwind schemes in shocked flow regions. We apply these hybrid schemes to various test problems and compare them with some conservative upwind schemes. The overall conclusion is that the hybrid upwind schemes are as accurate as the corresponding conservative schemes. The hybrid schemes are, however, more efficient.

1. INTRODUCTION

This work is concerned with *shock-capturing* schemes of *upwind* type for solving a system of conservation laws modelling one-dimensional two-phase flow in a pipeline. An accurate prediction of various two-phase flow phenomena is essential in many applications, ranging from internal combustion engines, via space vehicle propulsion systems and nuclear energy plants, to the design and operation of petroleum production systems. The so-called *drift flux* model considered in this paper is a two-phase flow model consisting of conservation equations for the two phases and one equation for the conservation of the momentum of the mixture. This model can be derived from the more fundamental two-fluid model (Ishii [6]) by adding together the momentum equations, thus obtaining one momentum equation for the mixture. To close the system of equations, a gas slip relation is provided. This relation must be determined on an experimental basis. The main advantages of the drift flux model are that the equations are in conservative form, which make them well suited for being discretized by conservative difference schemes, and that the model is hyperbolic, at least in a physically reasonable region of parameters, see, e.g., [2].

In general, the drift flux model has a very complex structure due to the fact that the submodels involved, e.g., density models, the empirical given slip relation and the frictional term, have a complex form and are often only given as empirical data. In addition, the gas slip relation may have a different shape for each of the flow regimes of interest and change with time, making the flux functions highly dependent on the space and time variables. Consequently, there is no algebraic expression of the fluxes as functions of the conservative variables. Even if the gas slip relation is given in purely algebraic form, the expressions for the fluxes as functions of the conservative variables are very complicated and not well suited for algebraic manipulations. In general, it is therefore very difficult to perform analytical calculations for the drift flux model. This fact implies that upwind schemes based on an algebraically given Riemann solver or a flux vector splitting are not easy to apply to the drift flux model. Fortunately, it is possible to construct fully numerical upwind schemes which avoid analytical computations, see Masella *et al.* [12], Romate [14], and [3]. Although these schemes are accurate, they tend to be very time consuming (see [3]). This is

Date: September 10, 1999.

Key words and phrases. Two-phase flow in pipelines, drift flux model, upwind scheme, primitive scheme, hybrid primitive-conservative scheme.

[a]RF-Rogaland Research, Thormølensgt. 55, N-5008 Bergen, Norway.
E-mail: Kjell-Kaare.Fjelde@rf.no.

[b]Department of Mathematics, University of Bergen, Johs. Brunsgt. 12, N–5008 Bergen, Norway.
E-mail: kenneth.karlsen@mi.uib.no.

mainly due to the need for repeatedly computing (numerically) the Jacobian of the system with respect to the conservative variables. Moreover, a conservative scheme will produce conservative variables at each new time level which must be transformed into primitive variables since the submodels involved are formulated in terms of primitive variables.

As will be discussed later, primitive formulations of the drift flux model have much simpler form than the conservative formulation and less coupled eigenstructure. Hence they could form a basis for developing more efficient upwind schemes for the drift flux model. However, it has by now become an accepted practice to use conservative schemes when solving hyperbolic conservation laws. There are many compelling reasons for doing this. Theoretically, the Lax-Wendroff theorem states if a conservative method converges, it does so to a weak solution of the conservation laws. Furthermore, if the scheme also satisfies an entropy condition, the converged solution is physically correct. On the other hand, it is easy to give examples which show that non-conservative (primitive) schemes converge to entirely non-physical solutions. In fact, Hou and LeFloch [5] have shown recently that non-conservative schemes (for a scalar equation) converge to a modified conservation law containing a measure source term. This source term is concentrated at the discontinuities, causing propagation of discontinuities at incorrect speeds, whereas it vanishes in regions where the solution is smooth. On the other hand, in [5] it was also proved that if the non-conservative schemes were locally corrected (in the vicinity of shocks) by using a conservative scheme, the resulting hybrid scheme would converge to the correct solution. This result may serve as a motivation for designing *hybrid* schemes for the drift flux model: use a cheap upwind scheme in smooth regions and switch to a more sophisticated upwind (shock-capturing) scheme near shocks.

Although sometimes equipped with a different motivation than us, hybrid schemes (for the Euler equations) have been considered recently by Harabetian and Pego [4] Karni [8, 9, 10], Ivings, Causon, and Toro [7], and Toro [17]. In this paper we follow the ideas of Toro [17], see also Ivings *et al.* [7] and Toro [16]. We consider hybrid primitive-conservative upwind schemes for the drift flux model which use a simple primitive upwind scheme in shock free regions and fully numerical and conservative upwind schemes in regions containing shocks. Concerning the primitive updates, we use a second order *MUSCL* scheme for non-conservative systems. This scheme utilises the three usual steps: (i) reconstruction, (ii) extrapolation, and (iii) evolution. In our implementation, the evolution step employs the solution of the Riemann problem for a linearized version of a primitive formulation of the drift flux model. Such a simple Riemann solver works very well for smooth flow since here the left and right states in the Riemann problem are close. For the conservative updates, we use either (i) a simple scheme based on an approximate-state Riemann solver with the approximate state being obtained from the primitive scheme or (ii) a fully numerical *Roe* scheme.

The difficulty in using the classical Roe scheme lies in the fact that one has to determine a Roe matrix ensuring conservation and correct recognition of shocks. Although such a matrix can be found analytically for, e.g., the Euler equations [13], it is difficult to construct such a matrix for general systems. In our case, a further restriction is set by the fact we want to allow for fairly general flux functions which may not even be given in algebraic form. Therefore we cannot hope to find analytical expression for the Roe matrix. Since the requirement is that the numerical schemes for the drift flux model must indeed be able to handle general flux functions, we have chosen to construct a matrix (numerically) by taking the original Jacobian evaluated at some average state and then modify its eigenvalues so that it satisfies Roe's conservation condition, thereby turning it into a true Roe matrix. This "trick" has been used recently by Romate [14], see also [3].

The rest of this paper is organized as follows: In §2, we present and discuss the drift flux model. In §3, the hybrid schemes are presented in detail. In §4, the numerical experiments are presented and discussed. Here the high-resolution hybrid schemes are applied to three main problems: (i) Shock tube problems. (ii) Propagation of pressure pulses. (iii) Transport of gas and liquid. The shock tube tests are classical and analytical solutions exist, whereas the remaining two problems are more complex and analytical computations are difficult. The hybrid schemes are compared against both primitive and conservative upwind schemes. Finally, in §5 we make some concluding remarks about hybrid schemes for the drift flux model.

Acknowledgements. This work has been carried out within the Well Flow group at RF-Rogaland Research. We thank Helge K. Dahle, Steinar Evje, Johnny Frøyen, Antonio Lage, Ove Sævareid and Erlend H. Vefring for discussions. In addition, we thank the Norwegian Research Council for financial support through the Strategic Institute Program "Complex Wells".

2. Two-Phase Flow — Drift Flux Model

Two-phase flow has applications within several areas and is known for being quite complicated both from a modelling and numerical point of view. Following Ishii [6], two-phase flow can be described by a one-dimensional two-fluid model involving six first order nonlinear partial differential equations describing mass, momentum and energy balances for each of the phases. This model is obtained from cross sectional averaging of the Navier-Stokes equations and replacing second order diffusion terms by empirical correlations which are flow regime dependent. The dynamics of two-phase flow is determined by these balance equations which involve complicated terms for interphase exchanges of mass, momentum and energy. In addition, wall friction and volumetric forces like gravity are highly responsible for the development of the flow.

The two-fluid model is widely used within the nuclear industry and it is well known that modelling of terms related to interphase exchanges is a difficult task. Another area of application for two-phase flow concerns, for example, production and transport of oil and gas through pipelines, which is an area of great importance for the oil industry. The fluids involved here are more complex and the two-fluid approach has usually been considered to be to complicated for practical use, although some commercial simulators have kept this approach, see, e.g., [1]. Instead one uses a simpler drift flux model obtained by adding together the momentum and energy equations for both phases, giving mixture equations for both momentum and energy. Difficult terms related to phase interaction cancel and the missing information must be replaced by an empirical given slip equation that relates the phase velocities. Source terms related to mass transfer, wall friction and volumetric forces are still present in the model.

Considering two-phase flow in pipelines it is convenient to identify three classes of physical phenomena, which all work on different time scales. These are interphase mass exchanges, fluid convection and propagation of pressure pulses (sonic waves). Mass transfer between the phases occurs on a very short time scale and shows up as stiff source terms in the mass conservation equations. Pressure pulses are mainly caused by flow rate changes and by valves which are quickly opened or closed. These waves have a time scale that are 10-100 times smaller than the transient behaviour of fluid transport. Considering the oil industry, it has been the dynamics of mass transport that traditionally has been of importance, while the fast sonic transients have been of major interest within the nuclear industry. Nevertheless, pressure pulses can also be of importance for the oil industry. Important applications include design of production systems, leak detection, and flow control. From a numerical point of view, the correct description of fluid transport and pressure waves requires high-resolution schemes possessing little numerical diffusion. In addition, it is important for the oil industry that the schemes can produce solutions within a reasonable amount of time.

The focus of this work is the numerical aspect and we will limit ourselves to consider gas-liquid flow in a long horizontal pipeline. The flow is assumed to be isothermal (no energy balance is needed) and there is no mass transfer between the phases. The one-dimensional drift flux model then takes the following form:

The mass conservation equation for the liquid phase

$$(\alpha_l \rho_l)_t + (\alpha_l \rho_l v_l)_x = 0. \tag{1}$$

The mass conservation equation for the gas phase

$$(\alpha_g \rho_g)_t + (\alpha_g \rho_g v_g)_x = 0. \tag{2}$$

The mixture momentum equation

$$(\alpha_l \rho_l v_l + \alpha_g \rho_g v_g)_t + (\alpha_l \rho_l v_l^2 + \alpha_g \rho_g v_g^2 + p)_x = -q. \tag{3}$$

In (1)-(2)-(3), t is time; x is the flow direction (space coordinate); p = is the pressure; α_ℓ is the volume fraction of phase $\ell = g, l$; ρ_ℓ is the density of phase $\ell = g, l$; v_ℓ is the velocity of phase $\ell = g, l$; and q represents the wall friction, The volume fractions α_l and α_g are related by $\alpha_l + \alpha_g = 1$. The conserved quantities in (1)-(2)-(3) represent the liquid mass, gas mass and mixture momentum. In addition, several closure laws must be given which involve density models for each phase, a slip relation and a model for wall friction. These models are usually quite complex and often given in tabular form based on experimental data. The main objective here is not to consider all these aspects but rather specify some simple models that can be used for the numerical test cases in §4.

First, we use a liquid density model of the form

$$\rho_l = \rho_{l,0} + \frac{p - p_{l,0}}{a_l^2}, \tag{4}$$

where $a_l = 1000$ [m/s] is the velocity of sound in the liquid phase and $\rho_{l,0}, p_{l,0}$ are given constants. We use a gas density model of the form

$$\rho_g = \frac{p}{a_g^2}, \tag{5}$$

where $a_g \approx 316$ [m/s] is the velocity of sound in the gas phase. For computational purposes, we will use the following gas slip relation given in purely algebraic form:

$$v_g = K v_{\text{mix}} + S, \tag{6}$$

where $v_{\text{mix}} = \alpha_l v_l + \alpha_g v_g$ is the mixture average velocity. This implies that in differential form $Dv_g = K_1 D\alpha_g + K_2 Dv_l$, where $K_1 = \frac{K(v_g - v_l)}{1 - K\alpha_g}$ and $K_2 = \frac{K\alpha_l}{1-K\alpha_g}$. A very simple model is used for the frictional pressure loss:

$$q = \frac{32 v_{\text{mix}} \mu_{\text{mix}}}{d^2}, \tag{7}$$

where d is the inner diameter of the tube and $\mu_{\text{mix}} = \alpha_l \mu_l + \alpha_g \mu_g$ is the mixture viscosity. The viscosities of the liquid and gas are, respectively, $\mu_l = 5 \cdot 10^{-2}$ [Pa $\cdot$ s] and $\mu_g = 5 \cdot 10^{-6}$ [Pa $\cdot$ s].

Note that if we let

$$U = \begin{pmatrix} \alpha_l \rho_l \\ \alpha_g \rho_g \\ \alpha_l \rho_l v_l + \alpha_g \rho_g v_g \end{pmatrix}, \quad F = \begin{pmatrix} \alpha_l \rho_l v_l \\ \alpha_g \rho_g v_g \\ \alpha_l \rho_l v_l^2 + \alpha_g \rho_g v_g^2 + p \end{pmatrix}, \quad Q = \begin{pmatrix} 0 \\ 0 \\ -q, \end{pmatrix},$$

then (1)-(2)-(3) can be written as a 3×3 system of conservation laws

$$U_t + F_x = Q. \tag{8}$$

Letting J denote the Jacobian of F with respect to the conservative variables U, we can write

$$U_t + JU_x = Q.$$

In general, it is difficult to express the flux function F in terms of conservative variables. The closure laws are formulated in terms of physical variables and, as mentioned before, often given in tabular form. It is therefore not possible to obtain explicit relations between the conservative and physical variables. Numerical schemes based on conservative variables will require some iterative procedure to transform these variables into physical variables for each calculation.

This leads us to consider other alternatives based on primitive formulations. One possible primitive formulation of the drift flux model is the following:

$$W_t + A(W)W_x = \tilde{Q}, \qquad A(W) = B^{-1}(W)C(W), \quad \tilde{Q} = B^{-1}(W)Q(W), \tag{9}$$

where $W = (\alpha_g, v_l, p)^{\mathrm{T}}$ is the vector of primitive variables and $A(W)$ is the coefficient matrix defined in terms of

$$B(W) := \begin{pmatrix} -\rho_l & 0 & \frac{\alpha_l}{a_l^2} \\ \rho_g & 0 & \frac{\alpha_g}{a_g^2} \\ \rho_g\, \alpha_g\, K_1 & \rho_l\, \alpha_l + \rho_g\, \alpha_g\, K_2 & 0 \end{pmatrix},$$

$$C(W) := \begin{pmatrix} -\rho_l\, v_l & \rho_l\, \alpha_l & \frac{v_l\, \alpha_l}{a_l^2} \\ \rho_g\, v_g + \rho_g\, \alpha_g\, K_1 & \rho_g\, \alpha_g\, K_2 & \frac{v_g\, \alpha_g}{a_g^2} \\ \rho_g\, \alpha_g\, v_g\, K_1 & \rho_l\, \alpha_l\, v_l + \rho_g\, \alpha_g\, v_g\, K_2 & 1 \end{pmatrix}.$$

Although it is possible to display the matrix $A(W)$ explicitly, we choose not do so here. For more complicated closure laws and when the parameters in the gas slip relation are given in tabulated form, it is still possible to determine the matrix $A(W)$ without computing (numerical) derivatives.

Mathematical properties of the system (1)-(3) were studied by Théron [15] and Benzoni-Gavage [2]. The model was shown to be hyperbolic in a physically reasonable region of parameters and three distinct and real eigenvalues were obtained under the main assumption that the liquid phase was considered incompressible. Two of the eigenvalues correspond to the rapid pressure waves propagating in the upstream and downstream direction of the fluid flow, while the last eigenvalue was associated to the gas volume waves and equal to the gas velocity. The characteristic fields corresponding to the sonic waves were shown to be genuinely nonlinear in the sense of Lax, while the last one is a linearly degenerate field. Further knowledge about the behaviour of the nonlinear pressure fields can be obtained by visualizing the sonic velocity as a function of the gas volume fraction shown, see Fig. 1. In particular, one should note that the acoustic velocity changes rapidly in the "one-phase to two-phase" transition regions, which give rise to strong nonlinear effects. It is also clear that the two-phase mixture has a lower sonic velocity than both pure liquid and gas.

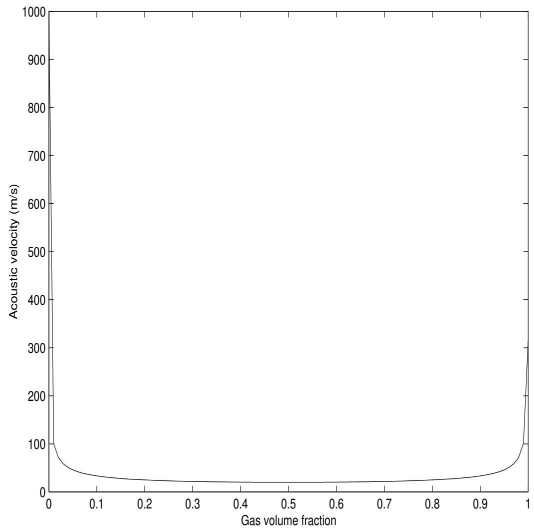

FIGURE 1. The acoustic velocity given from the eigenvalues as a function of α_g for the slip relationship $v_g = v_l$. The gas and liquid are in rest under atmospheric conditions.

3. Numerical Algorithm

In this section, we describe the hybrid upwind schemes for the drift flux model. We first describe the non-conservative (primitive) scheme and the conservative schemes. Then we describe a simple strategy for switching from the primitive scheme to a conservative scheme in the vicinity of shock waves. Finally, we say a few words about our treatment of boundary conditions.

To approximate the solution of (1)-(2)-(3), we introduce a mesh in the (x, t) plane where the spatial grid points are denoted by x_j and the time levels by t_n. We denote the spacing in the x and t variables by Δx and Δt, respectively. Approximate solutions in primitive and conservative variables are denoted respectively by W_j^n and U_j^n.

3.1. **Non-Conservative Updating.** With the basis in the primitive formulation (9), we shall here consider a non-conservative MUSCL scheme of the form (see Toro [17])

$$W_j^{n+1} = W_j^n - \frac{\Delta t}{\Delta x}\bar{A}_j\left[W_{j+1/2}^{n+1/2} - W_{j-1/2}^{n+1/2}\right] + \tilde{Q}_j^n. \tag{10}$$

where the intermediate states $W_{j\pm1/2}^{n+1/2}$ and the coefficient matrix $\bar{A}_j$ will be determined next. The basis of any MUSCL scheme (see van Leer [18, 19]) is the reconstruction of piecewise constant data into a piecewise linear distribution of the data. To this end, we introduce a piecewise linear function $W^n(x)$ defined by

$$W^n(x) = W_j^n + S_j\big(x - x_j\big), \qquad x \in (x_{j-1/2}, x_{j+1/2}), \tag{11}$$

where S_j denotes a suitable (limited) slope constructed from the given cell averages $\{W_j^n\}_j$ (see also Remark 3.1 below). The next step is to extrapolate the data to the edges of each cell, yielding the extrapolated values

$$W_j^l = W_j^n - \frac{\Delta x}{2}S_j, \qquad W_j^r = W_j^n + \frac{\Delta x}{2}S_j. \tag{12}$$

The extrapolated values W_j^l and W_j^r are then evolved half a time step according to the non-conservative formulas

$$\hat{W}_j^{l,r} = W_j^{l,r} - \frac{1}{2}\frac{\Delta t}{\Delta x}A_j^n\left[W_j^r - W_j^l\right], \qquad A_j^n = A(W_j^n). \tag{13}$$

Finally, in order to compute the intermediate state $W_{j+1/2}^{n+1/2}$, we need to find the self-similar solution $W_{j+1/2}(\xi)$, $\xi = (x - x_{j+1/2})/t$, of the Riemann problem

$$W_t + A(W)W_x = 0, \qquad W(x,0) = \begin{cases} W_l := \hat{W}_j^r, & \text{for } x \le x_{j+1/2}, \\ W_r := \hat{W}_{j+1}^l, & \text{for } x > x_{j+1/2}, \end{cases} \tag{14}$$

and set $W_{j+1/2}^{n+1/2} = W_{j+1/2}(0)$. We approximate the Riemann problem (14) by the linear Riemann problem

$$W_t + \hat{A}W_x = 0, \qquad W(x,0) = \begin{cases} W_l, & \text{for } x \le x_{j+1/2}, \\ W_r, & \text{for } x > x_{j+1/2}, \end{cases} \tag{15}$$

where

$$\hat{A} = A\Big(\frac{W_l + W_r}{2}\Big).$$

Note that this is a good approximation for smooth flow. We now solve the linear Riemann problem (15) exactly. To this end, we assume that the matrix $\hat{A}$ is diagonalizable so that it possesses an eigenvector basis. Let $\hat{\lambda}_1, \hat{\lambda}_2, \hat{\lambda}_3$ be eigenvalues of $\hat{A}$, and $\hat{R}_1, \hat{R}_2, \hat{R}_3$ and $\hat{L}_1, \hat{L}_2, \hat{L}_3$ the right and left eigenvectors respectively of $\hat{A}$ such that $\hat{L}_\ell \cdot \hat{R}_\kappa = \delta_{\kappa\ell}$ for $\kappa, \ell = 1, 2, 3$. The eigenvalues and eigenvectors of $\hat{A}$ can be found analytically. We consider the decomposition

$$W_r - W_l = \sum_{\ell=1}^{3} \hat{\alpha}_\ell \hat{R}_\ell, \qquad \hat{\alpha}_\ell = \hat{L}_\ell \cdot (W_r - W_l),$$

and let $W_k^{\mathrm{app}} := W_l + \sum_{\ell=1}^{k-1} \hat{\alpha}_\ell \hat{R}_\ell$, $k = 1, 2, 3, 4$. Then the self-similar solution $W_{j+1/2}^{\mathrm{app}}(\xi)$ of (15) can be written as

$$W_{j+1/2}^{\mathrm{app}}(\xi) = \begin{cases} W_1^{\mathrm{app}}, & \text{if } \xi < \hat{\lambda}_1, \\ W_2^{\mathrm{app}}, & \text{if } \hat{\lambda}_1 < \xi < \hat{\lambda}_2, \\ W_3^{\mathrm{app}}, & \text{if } \hat{\lambda}_2 < \xi < \hat{\lambda}_3, \\ W_4^{\mathrm{app}}, & \text{if } \xi > \hat{\lambda}_3, \end{cases}$$

Supposing that no eigenvalue $\hat{\lambda}_i$ vanishes at the interface $\xi = 0$, we now define

$$W_{j+1/2}^{n+1/2} := W_{j+1/2}^{\mathrm{app}}(0) = W_l + \sum_{\hat{\lambda}_\ell < 0} \hat{\alpha}_\ell \hat{R}_\ell = W_r - \sum_{\hat{\lambda}_\ell > 0} \hat{\alpha}_\ell \hat{R}_\ell. \tag{16}$$

There are various ways to calculate the coefficient matrix $\bar{A}_j$ (see [7, 17]). Here we will employ the simplest and most computational efficient choice

$$\bar{A}_j = A\Big(\frac{W^{n+1/2}_{j-1/2} + W^{n+1/2}_{j+1/2}}{2}\Big).$$

Remark 3.1. There exists a variety of limiters that can be used to calculate the slopes $\{S_j\}$ in the scheme described above. We refer to, e.g., [11, 16] for a detailed description of the available limiters. In this paper we will only use a few of them; namely, MINMOD, MC (Monotonized Centered), and SUPERBEE. MINMOD is the most diffusive limiter of the above limiters. This limiter selects the wave with the smallest norm of the two compared, provided the jumps across the waves are in the same direction, i.e., the wave strengths have common sign. If not, the wave is entirely suppressed. On the other hand, the SUPERBEE limiter is known to be overcompressive, i.e., it tends to sharpen profiles into discontinuities. The MC limiter lies somewhere between MINMOD and SUPERBEE and gives good results in most situations.

3.2. **Conservative Updating.** Explicit conservative schemes for solving (8) are based on the formula

$$U^{n+1}_j = U^n_j - \frac{\Delta t}{\Delta x}\Big[\mathcal{F}_{j+1/2} - \mathcal{F}_{j+1/2}\Big] + Q^n_j, \qquad \mathcal{F}_{j+1/2} = \mathcal{F}_{j+1/2}(U^n; j), \tag{17}$$

where U^n_j is an average of the conserved variables on the cell $(x_{j-1/2}, x_{j+1/2})$ centered around x_j and $\mathcal{F}_{j+1/2}$ is the numerical flux, which is determined by the particular scheme being used.

Note that a conservative version of the primitive scheme described in §3.1 is most easily obtained by computing the numerical flux in (17) as

$$\mathcal{F}_{j+1/2} = F\left(W^{n+1/2}_{j+1/2}\right), \tag{18}$$

where the intermediate state $W^{n+1/2}_{j+1/2}$ is defined in (16) This very simple conservative updating is related to the so-called approximate-state Riemann solvers in Toro [16].

We will next describe a fully numerical Roe scheme for the conservative updates. In Roe's original scheme [13], U^{n+1}_j is determined by taking the cell average of the exact solution of the linear Riemann problem

$$U_t + \hat{J}U_x = 0, \qquad U(x,0) = \begin{cases} U^n_j, & \text{for } x \le x_{j+1/2}, \\ U^n_{j+1}, & \text{for } x > x_{j+1/2}, \end{cases} \tag{19}$$

where the Roe matrix $\hat{J} = \hat{J}(U^n_j, U^n_{j+1})$ must satisfy the following conditions:

$$\begin{cases} \text{(i) } \hat{J}(U^n_j, U^n_{j+1}) \text{ has only real eigenvalues and is diagonalizable.} \\ \text{(ii) } F(U^n_{j+1}) - F(U^n_j) = \hat{J}(U^n_j, U^n_{j+1})(U^n_{j+1} - U^n_j). \\ \text{(iii) } \hat{J}(U^n_j, U^n_{j+1}) \to J(U) \text{ as } U^n_j, U^n_{j+1} \to U. \end{cases} \tag{20}$$

Condition (i) on hyperbolicity is an obvious requirement. Condition (iii) ensures consistency with the conservation laws (8). Condition (ii) ensures conservation and correct recognition of isolated discontinuities. Thanks to condition (ii) in (20), the Roe scheme can be written in conservative form (17). In what follows, we denote by $\hat{R}_1, \hat{R}_2, \hat{R}_3$ the right eigenvectors associated with the eigenvalues $\hat{\lambda}_1, \hat{\lambda}_2, \hat{\lambda}_3$ of the matrix $\hat{J}$, $\hat{\Lambda}$ the diagonal matrix which has as diagonal entries the eigenvalues of $\hat{J}$ and $\hat{R}$ the matrix of which the columns are the right eigenvectors of $\hat{J}$, and $|\hat{J}|$ the matrix $\hat{R}|\hat{\Lambda}|\hat{R}^{-1}$ where $|\hat{\Lambda}| = \mathrm{diag}(|\hat{\lambda}_1|, |\hat{\lambda}_2|, |\hat{\lambda}_3|)$. Note that if we decompose

$$U^n_{j+1} - U^n_j = \sum_{\ell=1}^{3} \hat{\alpha}_\ell \hat{R}_\ell,$$

then the numerical flux $\mathcal{F}_{j+1/2} = \mathcal{F}^{\mathrm{Roe}}_{j+1/2}$ for the Roe scheme can be written (see, e.g., [11])

$$\begin{aligned}\mathcal{F}^{\mathrm{Roe}}_{j+1/2} &= F(U^n_{j+1}) - \sum_{\hat{\lambda}_\ell > 0} \hat{\lambda}_\ell \hat{\alpha}_\ell \hat{R}_\ell = F(U^n_j) + \sum_{\hat{\lambda}_\ell < 0} \hat{\lambda}_\ell \hat{\alpha}_\ell \hat{R}_\ell \\ &= \frac{1}{2}\big(F(U^n_j) + F(U^n_{j+1})\big) - \frac{1}{2}\sum_{\ell=1}^{3} |\hat{\lambda}_\ell| \hat{\alpha}_\ell \hat{R}_\ell \\ &= \frac{1}{2}\big(F(U^n_j) + F(U^n_{j+1})\big) - \frac{1}{2}\big|\hat{J}(U^n_j, U^n_{j+1})\big|\big(U^n_{j+1} - U^n_j\big).\end{aligned} \tag{21}$$

The above approach leads to first order accuracy. Second order spatial and temporal accuracy can be accomplished by employing the MUSCL or Variable Extrapolation idea of van Leer [18, 19] (see also [11, 16]). We have chosen to do the reconstruction/extrapolation step as well as the evolution half-step with respect to primitive variables; that is, we use (12) and (13) to calculate the intermediate states $\hat{W}^{l,r}_j$. These variables are subsequently converted to conservative variables $\hat{U}^{l,r}_j$ using the closure laws. This approach makes it easier to formulate a hybrid scheme and omit recalculation of intermediate states for each conservative update. The numerical flux is given by

$$\mathcal{F}_{j+1/2} = \mathcal{F}^{\mathrm{Roe}}_{j+1/2}\Big(\hat{U}^r_j, \hat{U}^l_{j+1}\Big),$$

and the conservative update U^{n+1}_j is calculated via (17).

To apply Roe's scheme, one must analytically construct a Roe matrix. In particular, it is difficult to find a matrix $\bar{A}$ satisfying condition (ii). Following Romate [14], we shall here employ a fully numerical Roe solver that avoids the analytical part of the original Roe scheme. Instead of trying to find an average state $\tilde{U}_{j+1/2}$ so that the Jacobian $\tilde{J} = J(\tilde{U}_{j+1/2})$ satisfies the Roe condition (ii) in (20) (see [13]), one can first simply construct the matrix

$$\bar{J} = J\Big(\frac{W^n_j + W^n_{j+1}}{2}\Big).$$

The matrix $\bar{J}$ automatically satisfies (i) and (iii) in (20) but not (ii). To deal with the latter, we first decompose the Jacobian $\bar{J}$ as

$$\bar{J} = \bar{R}\bar{\Lambda}\bar{R}^{-1},$$

where $\bar{R}$ is the matrix of which the columns are the right eigenvectors of $\bar{J}$, and $\bar{\Lambda}$ is the diagonal matrix having the eigenvalues of $\bar{J}$ as diagonal entries. Next, we determine a diagonal matrix $\hat{\Lambda}$ such that

$$\bar{R}\hat{\Lambda}\bar{R}^{-1}\Delta U = \Delta F,$$

where $\Delta U = U^n_{j+1} - U^n_j$ and $\Delta F = F(U^n_{j+1}) - F(U^n_j)$. Then we define $\hat{J} = \hat{J}(U^n_j, U^n_{j+1})$ as

$$\hat{J} = \begin{cases} \bar{R}\hat{\Lambda}\bar{R}^{-1}, & \text{if } U^n_j \neq U^n_{j+1}, \\ \bar{R}\bar{\Lambda}\bar{R}^{-1}, & \text{if } U^n_j = U^n_{j+1}. \end{cases}$$

It is easily checked that the matrix $\hat{J}$ now satisfies the Roe condition (ii) in (20). Furthermore, conditions (i) and (iii) are also satisfied. Hence, $\hat{J}$ is a true Roe matrix satisfying all three conditions (i) - (iii) in (20). As is well known, it is often necessary to modify Roe's scheme in order to remove entropy violating shock waves. There exist various ways to do this (see, e.g., [16]), but it has not been found necessary to implement any of them in the present work.

Remark 3.2. For comparison purposes, we will also compute solutions using the *approximate-state Godunov* scheme and the *rough Gounov* scheme [12], which both fall into the class of conservative upwind schemes. The approximate-state Godunov scheme is defined by (17) and (18). The rough Godunov scheme, which is described and tested in [12], is based on solving the linear Riemann problem (19) with $\hat{J}$ determined by evaluating the Jacobian of F at some intermediate state. The numerical flux $\mathcal{F}_{j+1/2}$ is then calculated by evaluating the flux function F at the value taken by the solution of the linear Riemann problem along $x = x_{j+1/2}$. Second order accuracy is obtained by using the MUSCL idea and a two-stage Runge-Kutta time discretization.

3.3. **Switching Strategy.** As mentioned in the introduction, non-conservative schemes fail to produce correct solutions in the presence of shock waves. We therefore choose to switch from the primitive updating formula (10) to a conservative updating formula (17) in a cell j if the two neighbouring Riemann problems contain a shock wave travelling in the direction of mesh point j.

To be more precise, consider a grid point $x = x_j$ and two neighboring Riemann problems $W^{\text{app}}_{j-1/2}(\xi)$ and $W^{\text{app}}_{j+1/2}(\xi)$. Denote by $p^{\text{app}}_{j-1/2}$ and $p^{\text{app}}_{j+1/2}$ the solutions for the pressure along the interfaces $x = x_{j-1/2}$ and $x = x_{j+1/2}$, respectively. Let $\varepsilon > 0$ be a small positive number. Then the updating of the solution at $x = x_j$ is done with a conservative upwind scheme (17) if

$$\left| \frac{p^{\text{app}}_{j\pm 1/2}}{p^n_i} - 1 \right| > \varepsilon, \tag{22}$$

otherwise the updating is done with the primitive upwind scheme (10). The choice of ε is not too important. Experience indicates that any value in the range $(0, 0.1)$ gives good results. This is also consistent with the experience in [17, 7] with the Euler equations. The mechanism is as follows: If ε is too large, one may end up with computing shocks (of moderate strength) with the primitive scheme. On the other hand, smaller values of ε mean that the conservative scheme is used at more grid points than strictly necessary. The idea of switching to a conservative updating once a shock is detected in the pressure field is taken from Toro [17], see also Ivings *et al.* [7]. For other switching techniques, see Harabetian and Pego [4], Hou and LeFloch [5], and Karni [10].

One should note that for the Euler equations (as in [17, 7]), the pressure is constant across contact waves. This is not the case with the drift flux model (see, e.g., [2]). This implies that (22) can wrongly identify contact waves in the pressure field as shock waves and hence switch unnecessarily from primitive to conservative updating. Having said this, in our experience the strength of the contact waves in the pressure field is very small, and they are thus rarely (wrongly) identified by (22) as shock waves, at least if ε is not too small. In fact, among all the numerical experiments that we have conducted (many not reported here), the largest pressure contact jumps encountered so far are those seen in the shock tube problems presented in §4.1. Even for these (in some sense unrealistic) examples, the test (22) did not wrongly identify the contact waves in the pressure field as shock waves. For the applications that we have in mind, we believe that the switching technique (22) is fairly robust. Nevertheless, we will in future work investigate alternative switching strategies.

3.4. **Boundary Treatment.** The hyperbolic nature of the model makes it important to treat correctly the information going in and out of the system. Without going into details, let us say that the treatment of the boundary conditions takes into account the information going out of the system through a set of compatibility relations [2], which are solved together with the imposed boundary conditions using upwind discretization. The obtained values at the boundary determine the boundary fluxes at the next time level. Considering the test cases studied here, the imposed conditions will typically be to specify some mass flow rates at the inlet of the pipeline and keep the pressure at atmospheric conditions at the outlet.

4. Numerical Results

In this section we present and discuss three numerical examples. The main purpose is to reveal the behaviour of the hybrid upwind schemes as well as comparing them against some high-resolution conservative upwind schemes. In the first example, we consider some simplified two-phase shock tube problems which are almost identical to the ones constructed in [2]. In the second example, we consider pressure pulse propagation for a constructed case and examine if there are large differences between the hybrid and conservative approaches regarding the description of these waves. In the third example, we consider the slower transient of liquid and gas transport in a pipeline. For the applications that we eventually have in mind, it is absolutely crucial that the hybrid approach describes mass transport properly.

The Jacobian of F (with respect to the conservative variables) is constructed analytically in the shock tube problems. For both the pressure pulse example and the liquid and gas transport example, we use (for simplicity) a no-slip relationship $v_g = v_l$. For the no-slip relationship it is still possible to construct the Jacobian analytically. However, to get an impression of how expensive the different schemes would be if more complicated closure laws were supplied, we have chosen to compute the Jacobian numerically.

4.1. **Shock Tube Problems.** A simplified drift flux model is considered which employs a constant liquid density $\rho_l = 1000$ [kg/m^3] and gas density given by (5). The gas slip parameters in (6) are given $K = 1.07$ and $S = 0.216$ [m/s]. The wall friction q is neglected, so that the model is without source term. For all the shock tube cases, a 100 [m] long horizontal pipe is considered which initially is separated in a left and right state at $x_0 = 50$ [m]. These states will be varied to obtain either rarefaction waves or shock waves in the first and third characteristic family.

For the numerical calculations, the primitive scheme, the hybrid scheme, and the conservative fully numerical Roe schemes have been tested. The hybrid scheme uses the Roe scheme for conservative updating and a switch (22) based on $\varepsilon = 0.01$. Notice that for these shock tube tests, some misplacement of the shock locations and changes in the left and right shock states should be expected for the primitive scheme. All schemes used a CFL number of 0.8 and space discretization $\Delta x = 0.5$ [m]. The MINMOD limiter was used to obtain second order accuracy in space.

4.1.1. *CASE–S1S3.* The left and right states for this Riemann problem are ($\alpha_{g,L} = 0.55$, $v_{l,L} = 10.37$ [m/s], $p_L = 80450$ [Pa], $\alpha_{g,R} = 0.55$, $v_{l,R} = 0.561$ [m/s], $p_R = 24282$ [Pa]).

The exact solution is composed of a 1-shock, a 2-contact discontinuity and a 3-shock. The results given by the different schemes at time $t = 1.0$ [s] are shown in Figs. 2-4. We have chosen to present plots of the gas volume fraction, liquid velocity and pressure. As anticipated, the primitive scheme produces shock waves with wrong strength. The shock positions are incorrect, but not very different from those predicted by the conservative scheme. The hybrid scheme used conservative updating both for the left- and right-going shock, and the solution was corrected. A closer look at the pressure curves reveals a small jump in pressure for the contact discontinuity which was discussed in §3.3. The hybrid scheme used primitive updating for this discontinuity, and the switching strategy seems to work well in identifying only nonlinear shocks for conservative updating. This conclusion is also valid for the Riemann problems presented below.

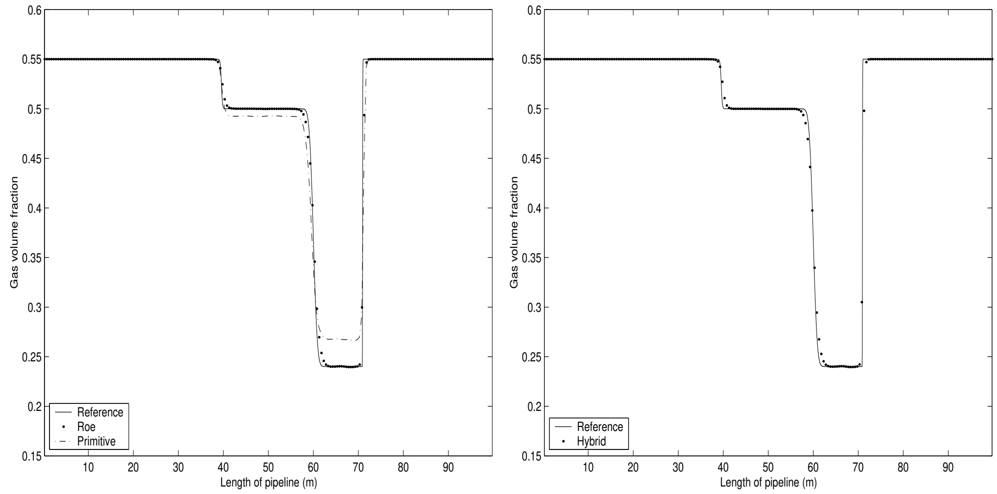

FIGURE 2. CASE–S1S3. Left: Primitive scheme VS Roe scheme. Right: Hybrid scheme.

4.1.2. *CASE–R1R3.* The left and right states of this Riemann problem are ($\alpha_{g,L} = 0.35$, $v_{l,L} = 1.868$ [m/s], $p_L = 192170$ [Pa], $\alpha_{g,R} = 0.30$, $v_{l,R} = 14.47$ [m/s], $p_R = 196690$ [Pa]).

The exact solution is composed of a 1-rarefaction, a 2-contact discontinuity and a 3-rarefaction. The results obtained at time $t = 1.0$ [s] are given in Figs. 5-7. As anticipated there were no significant differences between the primitive and conservative approach. The hybrid scheme invoked a few conservative updates in the beginning since the rarefaction waves had a sharp gradient then.

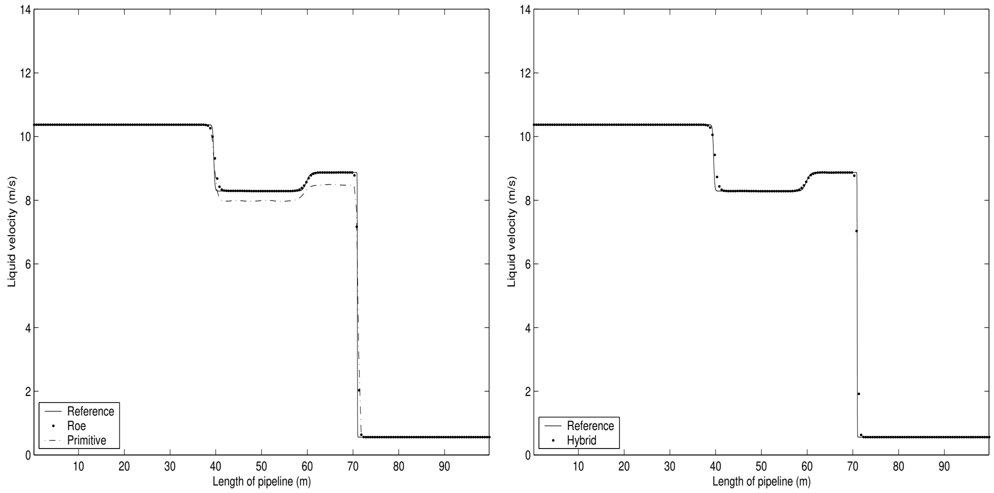

FIGURE 3. CASE–S1S3. Left: Primitive scheme VS Roe scheme. Right: Hybrid scheme.

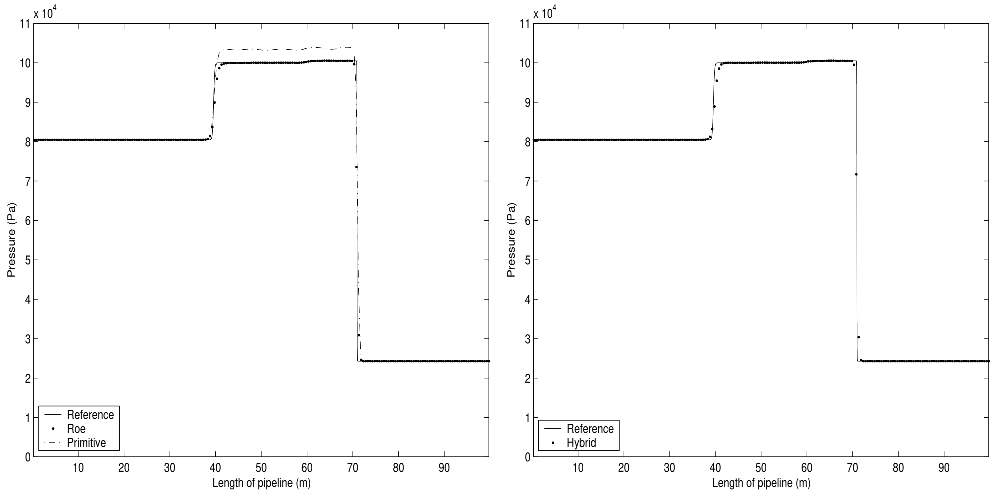

FIGURE 4. CASE–S1S3. Left: Primitive scheme VS Roe scheme. Right: Hybrid scheme.

4.1.3. *CASE–R1S3.* The left and right states are in this case ($\alpha_{g,L} = 0.2$, $v_{l,L} = 0.37$ [m/s], $p_L = 274830$ [Pa], $\alpha_{g,R} = 0.6$, $v_{l,R} = 3.48$ [m/s], $p_R = 58771$ [Pa]).

The exact solution is composed of a 1-rarefaction, a 2-contact discontinuity and a 3-shock. The results given by the numerical schemes at time $t = 1.0$ [s] are shown in Figs. 8-10. The solution provided by the primitive scheme is almost equal to that given by the conservative approach. The hybrid scheme invoked conservative updates for the shock.

4.1.4. *CASE–S1R3.* The left and right states are ($\alpha_{g,L} = 0.7$, $v_{l,L} = 10.896$ [m/s], $p_L = 76542$ [Pa], $\alpha_{g,R} = 0.4$, $v_{l,R} = 15.12$ [m/s], $p_R = 192020$ [Pa]).

The exact solution is composed of a 1-shock, a 2-contact discontinuity and a 3-rarefaction. The results after time $t = 1.0$ [s] are shown in Figs. 11-13. Also this example reveals very small differences between the primitive and conservative scheme. The hybrid scheme invoked conservative updates for the left-going shock.

4.1.5. *CASE–FAST–S1S3.* The left and right states of the final Riemann problem are ($\alpha_{g,L} = 0.55$, $v_{l,L} = 24.84$ [m/s], $p_L = 523200$ [Pa], $\alpha_{g,R} = 0.55$, $v_{l,R} = 1.70$ [m/s], $p_R = 804300$ [Pa]).

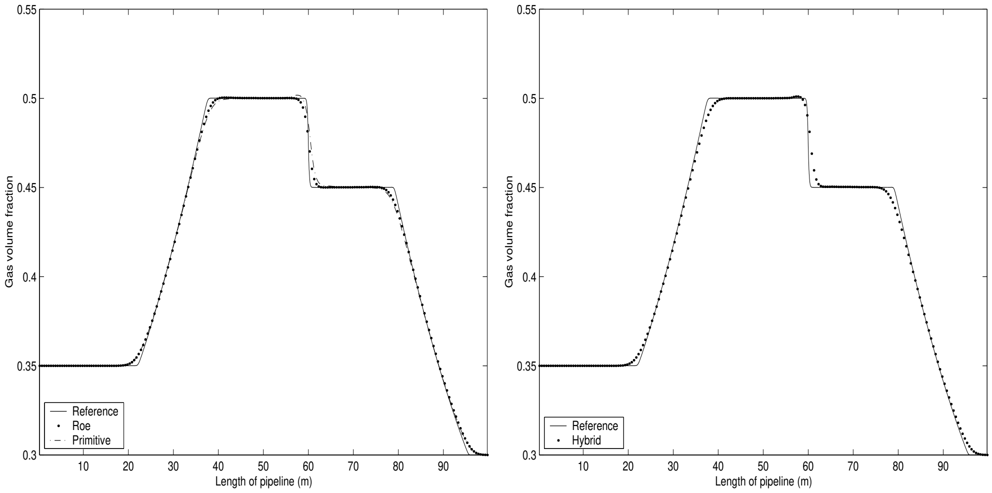

FIGURE 5. CASE–R1R3. Left: Primitive scheme VS Roe scheme. Right: Hybrid scheme.

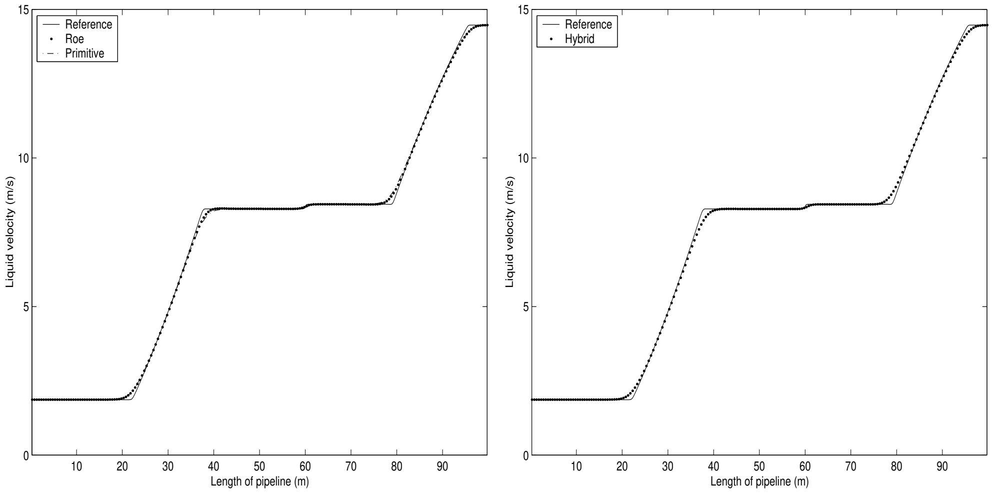

FIGURE 6. CASE–R1R3. Left: Primitive scheme VS Roe scheme. Right: Hybrid scheme.

The initial pressure is somewhat higher in this example than in §4.1.1, which increases the velocity of the nonlinear pressure waves. The exact solution is composed of a 1-shock, a 2-contact discontinuity and a 3-shock. The solutions given by the schemes after time $t = 0.6$ [s] are shown in Figs. 14-16. Some differences are observed concerning the shock strengths, while the shock positions are not that different. The hybrid scheme used conservative updating for both shocks and the solution was corrected.

4.2. **Propagation of Pressure Pulses.** We consider a 1000 [m] long horizontal pipeline with diameter 10 [cm]. The first 750 meters are filled with pure stagnant liquid while the last 250 meters are filled with 99% liquid and 1% gas. The pressure is initially 1 [bar] in the pipeline. We are interested in simulating a pressure pulse generated by increasing the inlet liquid rate from 0 to 0.3 [kg/s] in 0.0025 [s]. If we recall §2 (see Fig. 1), we notice that the speed of sound is 1000 [m/s] in the pure liquid region, but as the two-phase region appears this drops dramatically. In the 1% gas region the speed of sound is approximately 100 [m/s]. Pressure waves entering the two-phase region from the one-phase region will create a strong shock since the corresponding eigenvalues experience a very rapid decrease. In what follows, the different schemes used a CFL number of 0.25

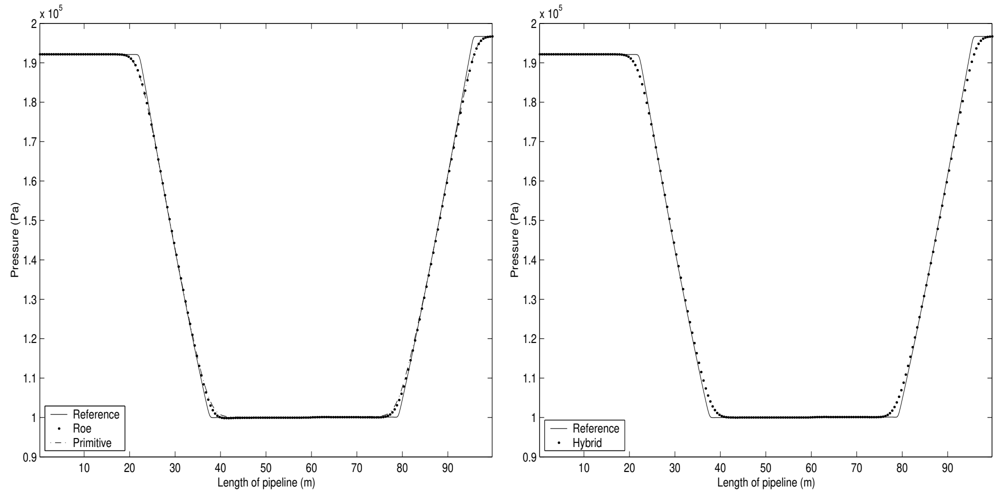

FIGURE 7. CASE–R1R3. Left: Primitive scheme VS Roe scheme. Right: Hybrid scheme.

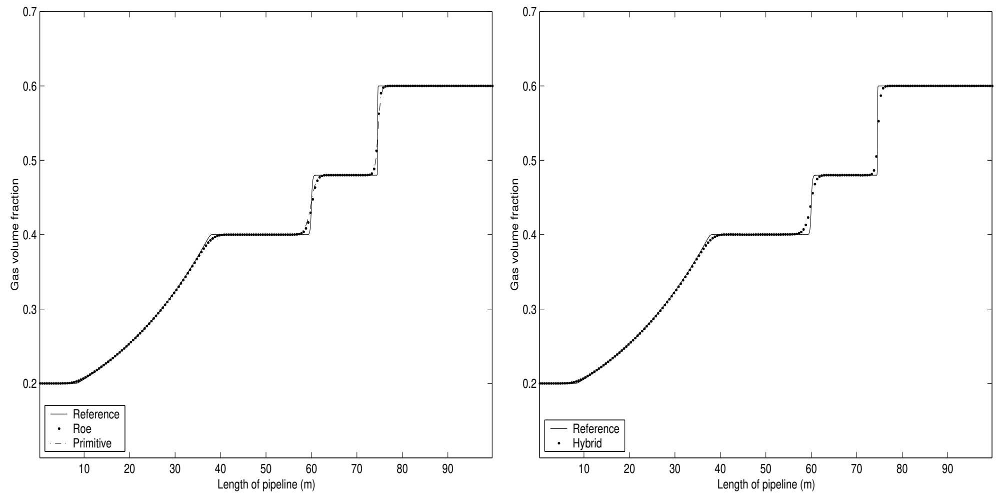

FIGURE 8. CASE–R1S3. Left: Primitive scheme VS Roe scheme. Right: Hybrid scheme.

and a space discretization $\Delta x = 10$ [m]. The MC (Monotonized Centered) limiter was used. We have tested the fully numerical Roe scheme, the rough Godunov scheme, the approximate-state Godunov scheme, the primitive scheme, and the hybrid scheme based on the approximate-state Godunov scheme for the conservative updates. The results are shown in Figs. 17-22.

The "instantaneous" increase of the inlet liquid flow rate generates a right-going pressure wave of amplitude 0.4 [bar]. In the pure liquid region this constitutes a weak shock since the characteristics of the 3rd family run almost in parallel. As shown in Fig. 17, the position of the pressure pulse at $t = 0.4$ [s] given by the primitive scheme seems to have the same position as the reference solution. When the two-phase region is reached a large part of the pulse will be reflected due to changes in the mixture density and acoustic velocity. The reflected pulse will be a rarefaction wave, but this is not easily seen since the corresponding characteristics run almost in parallel. In addition, a strong shock will form which continues to travel to the right in the two-phase region with a strongly reduced velocity. As one would expect, the position of this shock (at times $t = 0.9$ [s] and $t = 1.3$ [s]) given by the primitive scheme is clearly misplaced and the left and right shock states are different from those obtained by the reference solution, see Figs. 17 and 22.

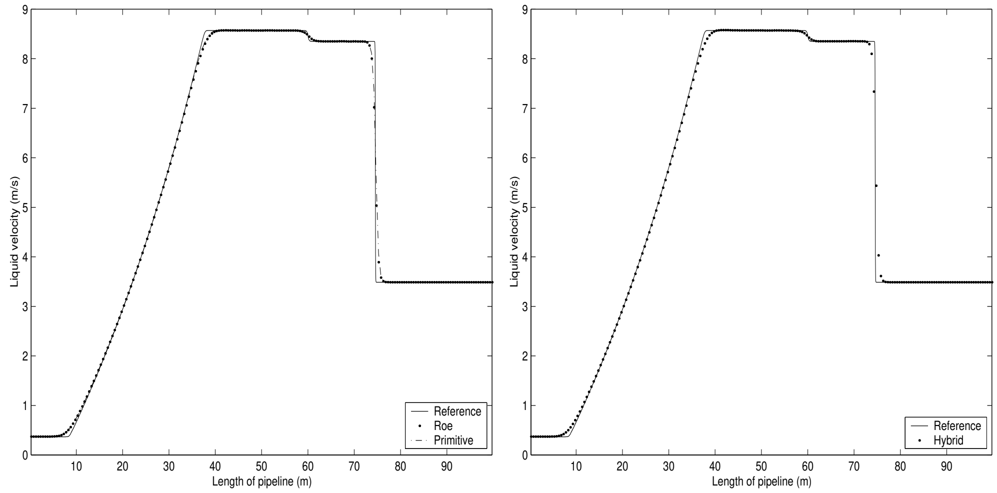

FIGURE 9. CASE–R1S3. Left: Primitive scheme VS Roe scheme. Right: Hybrid scheme.

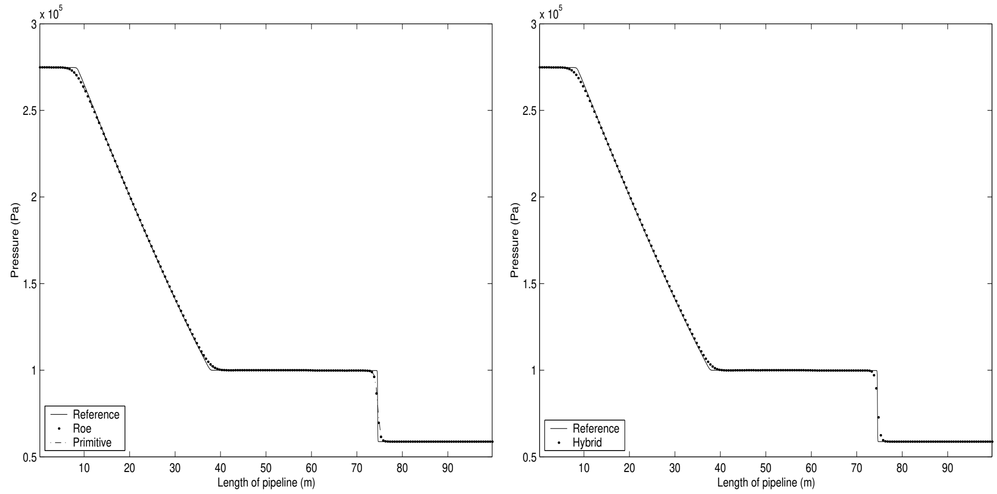

FIGURE 10. CASE–R1S3. Left: Primitive scheme VS Roe scheme. Right: Hybrid scheme.

The solutions obtained by the Roe scheme are shown in Fig. 18. We only mention that they seem to be in good agreement with the reference solutions. The results obtained by the rough Godunov scheme are shown in Fig. 19. Here we notice that the reflected pulse is having a rather strange behaviour and seems to be misplaced. In addition, the intermediate state between the two pulses is different from the one in the reference solution. Although we are not completely sure, this may be related to the fact that the numerical flux in the rough Godunov scheme is not continuous when an eigenvalue experiences a change of sign, see [12].

The results obtained by the approximate-state Godunov scheme are shown in Fig. 20, see also Fig. 22. Although the waves propagating in the one-phase region are somewhat less diffusive, the results obtained are quite similar to those obtained by the Roe scheme (compare with Fig. 18).

The results obtained by the hybrid scheme are shown in Fig. 21. Compared to the primitive scheme (see Fig. 17), the position of the strong shock is corrected and the shock states are well predicted. The switch (22) between the conservative and primitive scheme used $\varepsilon = 0.01$. A

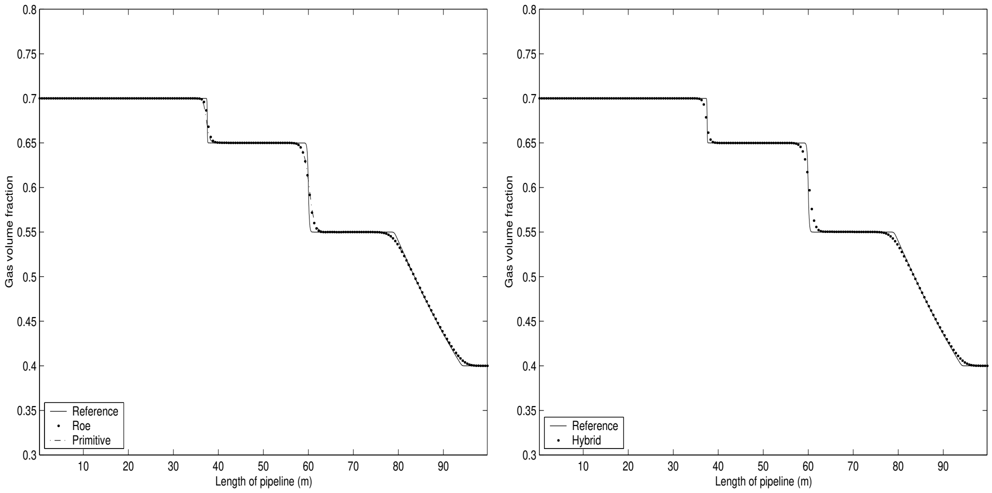

FIGURE 11. CASE–S1R3. Left: Primitive scheme VS Roe scheme. Right: Hybrid scheme.

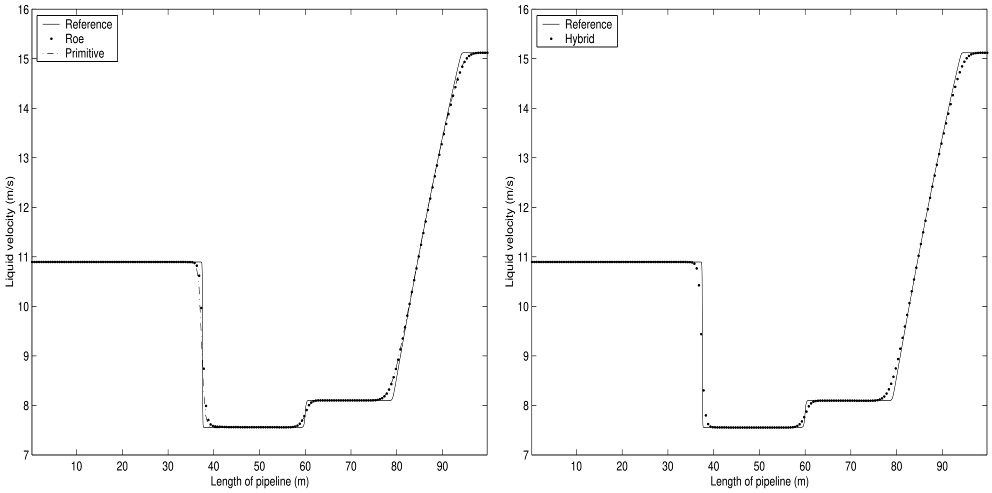

FIGURE 12. CASE–S1R3. Left: Primitive scheme VS Roe scheme. Right: Hybrid scheme.

conservative update was invoked, however, both for the right-going shock and the reflected left-going rarefaction wave. The reason for this is that the "gradient" of the shock and the gradient of the rarefaction wave both are of same magnitude for this example.

A final comment to be made is the decrease of the amplitude of the pressure pulse as a function of the position. In Fig. 18, it is seen that the pulse at $t = 0.4$ [s] has a decreased amplitude due to physical attenuation caused by the frictional forces. This must not be confused with the situation at $t = 1.3$ [s] where the inlet pressure is even higher than initially. This is also caused by the frictional terms since the liquid velocity has increased after the reflection. The pressure at a given point depends on both frictional forces and pressure waves, but the amplitude of the pressure waves are always subdued by the frictional forces. In most applications, the frictional pressure is dominating and the pressure waves appear as small perturbations of the total pressure.

4.3. **Transport of gas and liquid.** We consider a horizontal pipeline with the same geometrical data as in the previous example. Initially, the pipe is filled with stagnant liquid and we are interested in modelling the transient behaviour induced by injecting gas and liquid at the inlet.

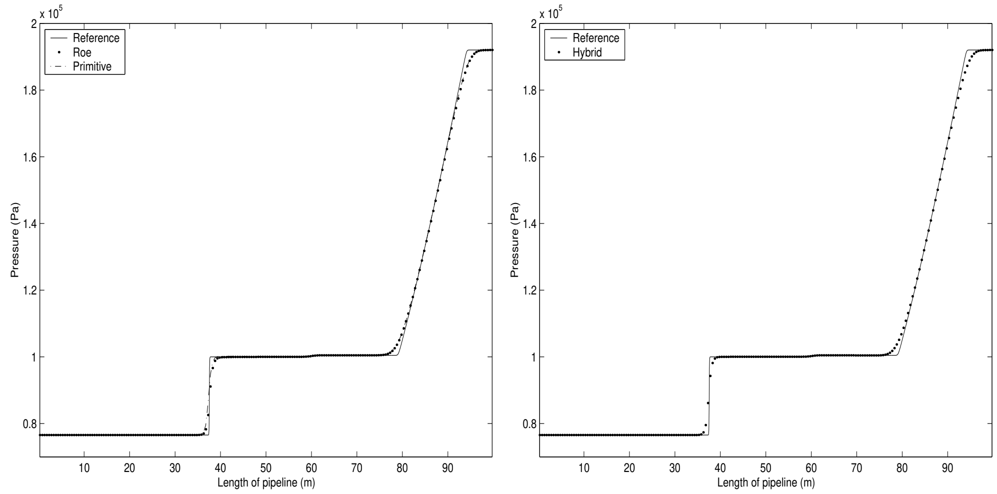

FIGURE 13. CASE–S1R3. Left: Primitive scheme VS Roe scheme. Right: Hybrid scheme.

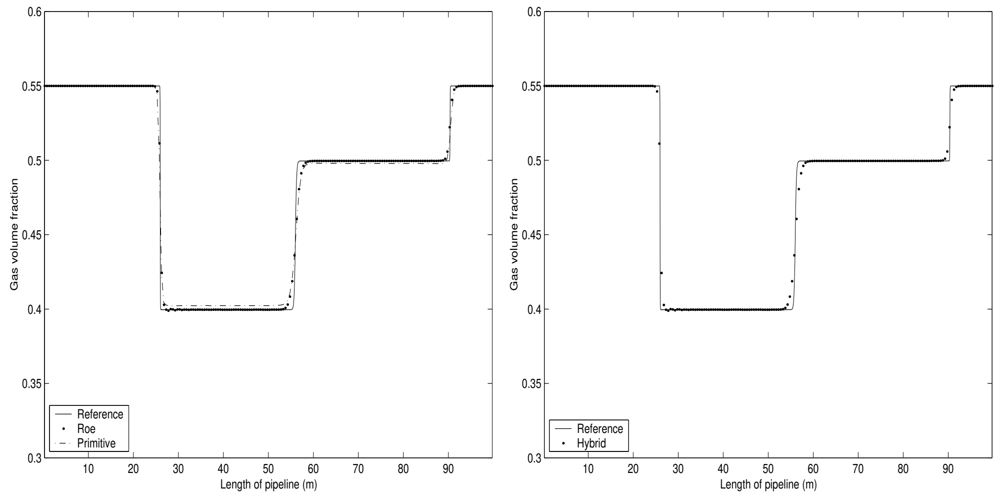

FIGURE 14. CASE–FAST–S1S3. Left: Primitive scheme VS Roe scheme. Right: Hybrid scheme.

The gas and liquid mass flow rates are increased to respectively 0.02 [kg/s] and 3.0 [kg/s] in 10 [s]. At the outlet boundary, the pressure is kept constant equal to 1 [bar].

The numerical calculations were performed with the fully numerical Roe scheme, the rough Godunov scheme, the approximate state Godunov scheme, the primitive scheme, and hybrid schemes using the Roe scheme and the approximate state Godunov scheme for the conservative updates. The choice of an appropriate switch is discussed below. All schemes applied the compressive SUPERBEE limiter, a CFL number of 0.5, and space discretization, $\Delta x = 20$ [m].

Figs. 23-26 show the time evolution of liquid and gas mass flow rates at the four positions $x = 250$ [m], 500 [m], 750 [m], 1000 [m] given by the different numerical schemes and the reference solution (solid line). In Figs. 27-28, the time evolution of pressure at $x = 0$ [m], 250 [m], 500 [m], 750 [m] is shown. Considering the pressure curves, a sharp peak is observed when the final inlet mass flow rates are obtained at time $t = 10$ [s]. This behavior is caused by the acceleration terms which are responsible for the pressure pulses. The peak is sharper at the inlet of the pipe since larger part of stagnant liquid must be set in motion. This peak vanishes after a short while, and mainly the frictional forces are responsible for the pressure development afterwards. As the gas and liquid

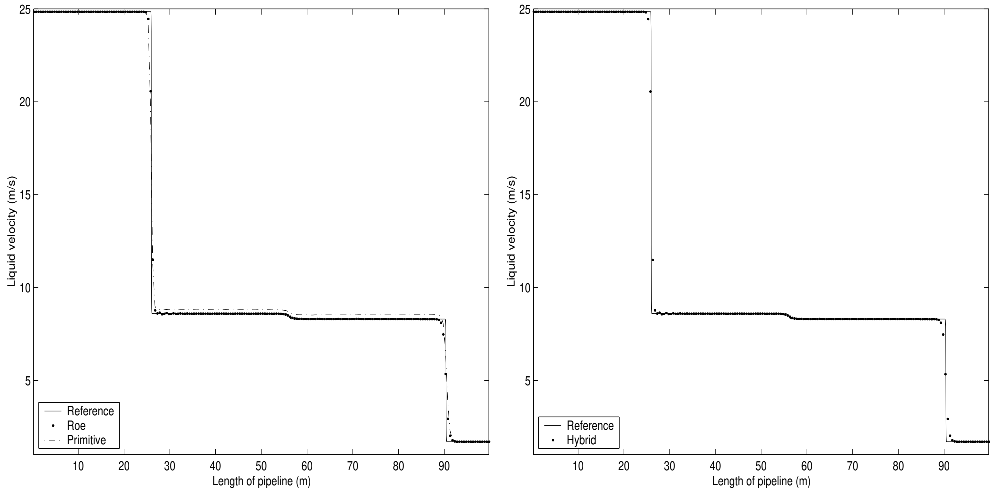

FIGURE 15. CASE–FAST–S1S3. Left: Primitive scheme VS Roe scheme. Right: Hybrid scheme.

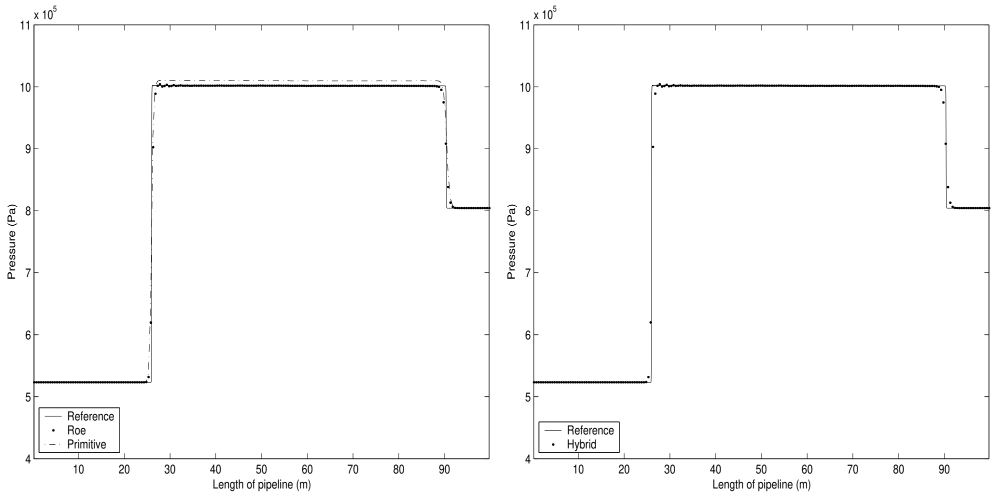

FIGURE 16. CASE–FAST–S1S3. Left: Primitive scheme VS Roe scheme. Right: Hybrid scheme.

propagate through the pipe they experience a decreasing pressure which causes the gas to expand. This expansion results in increased gas mass flow rates, and the liquid in front of the gas is moved with larger velocities. The liquid mass flow rate at a given position increases until the gas passes and drops quickly afterwards. The gas mass rate increases rapidly when the gas arrives, and this scenario becomes more extreme when the gas reaches the outlet where the gas flow rate forms a sharp peak which drops quickly towards the steady state solution. The increased velocities caused by gas expansion result in a larger frictional pressure loss and as observed in, e.g., Fig. 27, the pressure at 250 [m], 500 [m], 750 [m] has a maximum when the gas passes these positions. Afterwards, the pressure starts to decrease slowly until the gas and liquid rates at the outlet have reached their maximum values and the pressure drops quickly to the steady state situation. This sharp decrease causes some gas expansion in the interior of the pipe and is responsible for the final peaks in the mass flow rates observed at $x = 250$ [m], 500 [m], 750 [m] (see Figs. 23-26). After approximately 800 [s], the flow has stabilized and the final steady state conditions are reached.

The mass flow rates predicted by the different schemes are quite similar (see Figs. 23-26). Even the primitive scheme gives flow rates which are in accordance with the reference solution.

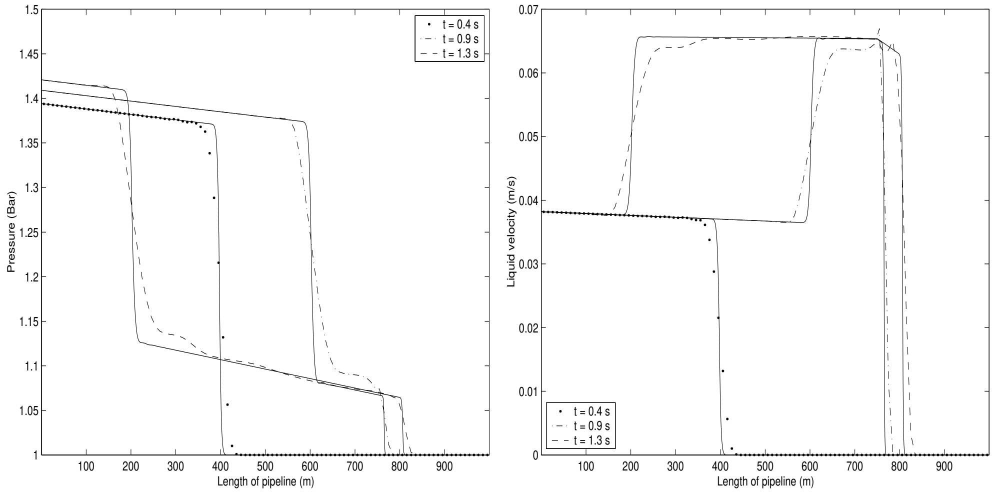

FIGURE 17. Primitive scheme. Left: Pressure pulse positions at three different times. Right: The corresponding liquid velocities. Reference solution is shown as solid line.

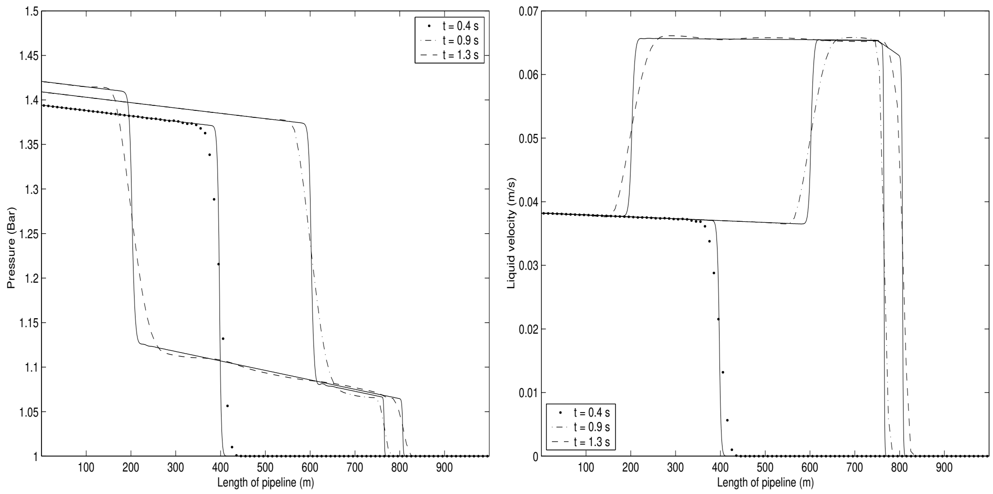

FIGURE 18. Roe scheme. Left: Pressure field at three different times. Right: The corresponding liquid velocities. Reference solution is shown as solid line.

The dynamics of mass transport is mainly determined by the frictional forces, and the mass (gas volume) waves are linear in nature and therefore well predicted by the primitive approach. Considering the pressure curves, a closer look at the peak generated by the pressure pulses reveals some differences between the primitive and conservative approaches, see Fig. 29. Notice that the fluctuations observed are caused by reflection of the pressure pulses at the boundaries and the magnitudes of these are somewhat different. As time passes, the frictional forces will attenuate these waves and both schemes end up with predicting the same pressure (see Fig. 29). In Fig. 30, a hybrid scheme with $\varepsilon = 0.01, 0.0075$ is used and the amplitudes are more in accordance with the reference solution. Unfortunately these choices of ε seem to invoke unnecessarily many conservative updates especially after the pressure pulses are subdued. The frictional pressure loss gradient becomes sharper as time passes and (22) is easily fulfilled even if there is no shock in the solution. This leads us to use a small ε in periods of flow rate changes and use a larger value when the corresponding pressure pulses are subdued to omit further unnecessary conservative updating.

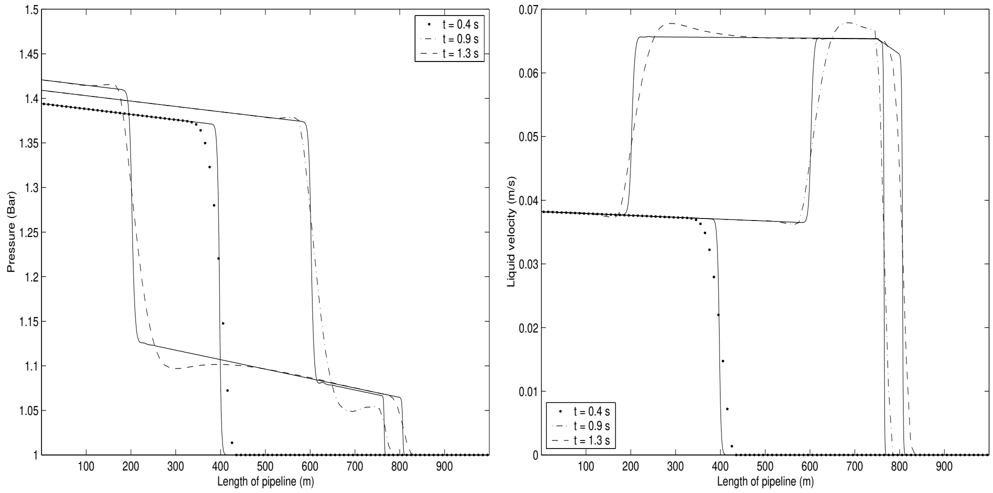

FIGURE 19. Rough Godunov scheme. Left: Pressure field at three different times. Right: The corresponding liquid velocities. Reference solution is shown as solid line.

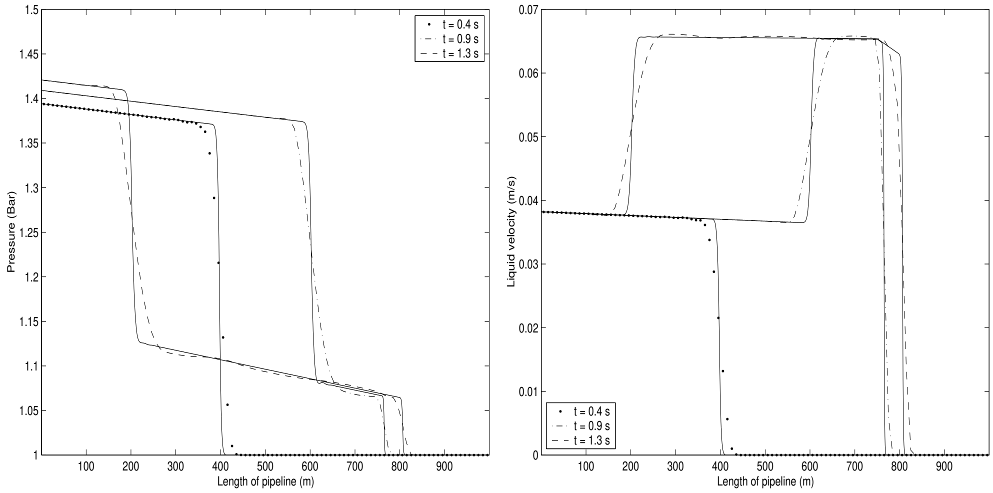

FIGURE 20. Approximate-state Godunov scheme. Left: Pressure field at three different times. Right: The corresponding liquid velocities. Reference solution is shown as solid line.

Based on this we chose to use $\varepsilon = 0.0075$ up to 40 [s] and $\varepsilon = 0.05$ afterwards. The results given by these hybrid scheme are shown in Figs. 31-33.

In Table 1, rough estimates of the CPU-time for the different schemes are given. The conservative approximate-state Godunov scheme, the primitive scheme, and the hybrid schemes turned out to be most efficient, mainly because numerical computation of the Jacobian is omitted. The approximate-state Godunov scheme was even cheaper than the primitive scheme since the conservative updating (17) is less expensive than the primitive update (10) where the primitive Jacobian has to be recalculated. The transformation between conservative and primitive variables needed in the conservative scheme is not that expensive for the submodels considered here, but more complex models would increase the computational costs and we may expect that the primitive scheme will turn out better in comparison for such cases. The other conservative schemes, the fully numerical Roe scheme and the rough Godunov scheme, were rather expensive, especially

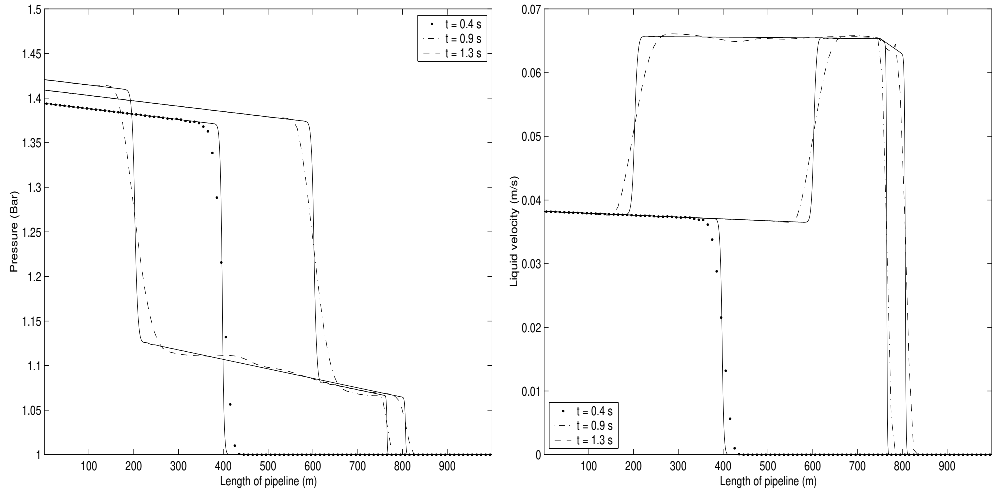

FIGURE 21. Hybrid scheme. Left: Pressure pulse positions at three different times. Right: The corresponding liquid velocities.

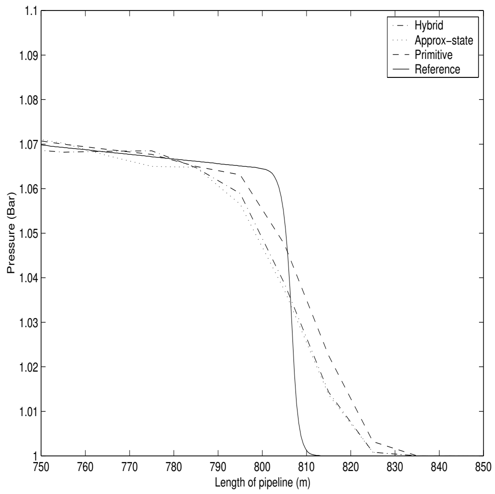

FIGURE 22. A closer look at the strong shock propagating to the right at $t = 1.3$ [s]. Here it is easier to see how the primitive scheme misplaces the shock while the hybrid scheme has correct shock description.

the latter since the Jacobian is calculated numerically twice at each time level (two-stage Runge-Kutta discretization). We notice that the CPU-time of the conservative Roe scheme were reduced drastically when the scheme was used in a hybrid fashion.

5. Conclusions

We have constructed and tested hybrid upwind schemes for the drift flux model. These schemes employ a very simple primitive upwind (MUSCL) scheme in smooth flow regions and more complex conservative upwind schemes in regions containing shocks. For the conservative updates, a fully numerical Roe scheme and an approximate-state Godunov scheme were tested. Both the corresponding hybrid schemes produced good results for all test cases. Concerning the case of mass transport (see §4.3), the fully primitive scheme also produced fairly good results. We expect, however, that for flow rate changes and other operational conditions which produce pressure pulses, there will be some differences between the conservative and primitive approach due to the

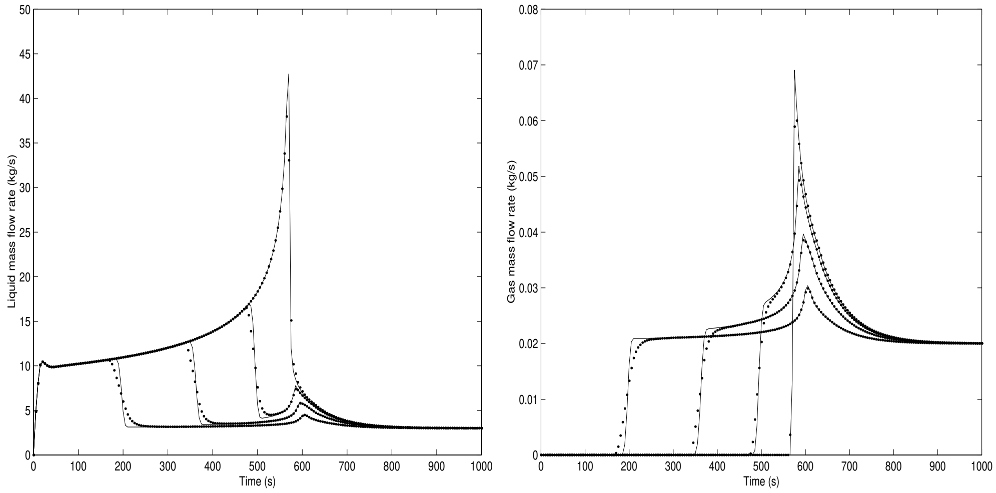

FIGURE 23. Roe scheme. Mass flow rates for positions $x = 250$ [m], 500 [m], 750 [m], 1000 [m] (from left to right in the plots). Left: Liquid mass flow rates. Right: Gas mass flow rates. Reference solution is shown as solid line, while approximate solution is shown as thick dots.

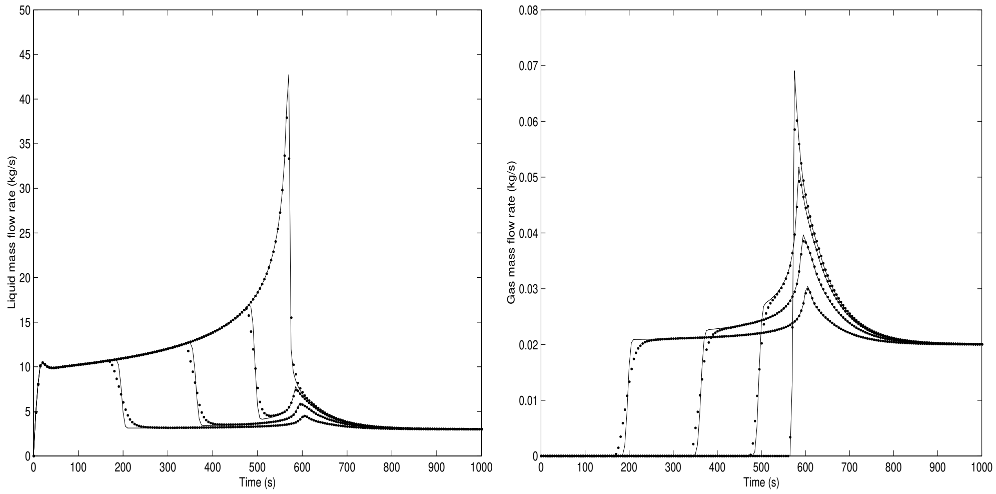

FIGURE 24. Rough Godunov scheme. As in Fig. 23, liquid (left) and gas (right) flow rates are plotted at four different positions as functions of time.

nonlinear behaviour of these waves. On the other hand, these differences will most likely disappear at later times since these pulses are attenuated by frictional forces.

We believe that the hybrid approach represents an interesting and useful way of "speeding up" conservative (and often fully numerical) upwind schemes for the drift flux model. As an example (see §4.3), let us recall that the computation time of the hybrid-Roe scheme was reduced significantly compared to the fully conservative Roe scheme, which here is mainly due to the fact that the (expensive) numerical calculation of the Jacobi matrix is needed by the hybrid-Roe scheme only in the (few) grid cells containing shocks. We also observed that the (conservative) approximate-state Godunov scheme, which uses the the primitive formulation to calculate the approximate states, is also quite cheap. However, for more complex submodels the transformation between conservative and primitive variables will be more expensive and we expect the hybrid approach to be more efficient in comparison since the number of transformations is highly reduced.

The switching strategy (22) used here, which essentially tries to detect nonlinear pressure waves (shocks), seems to work well. We expect, however, that it will depend very much on

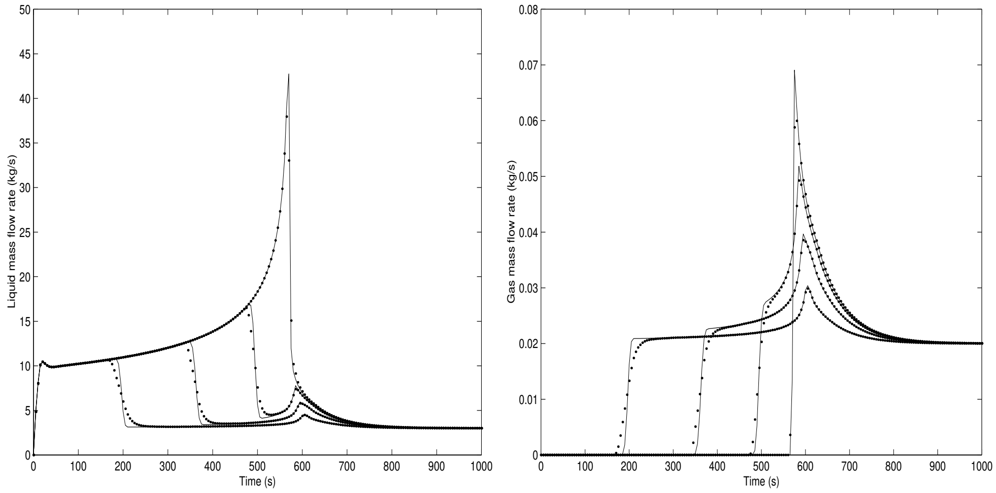

FIGURE 25. Approximate-state Godunov scheme. As in Fig. 23, liquid (left) and gas (right) flow rates are plotted at four different positions as functions of time.

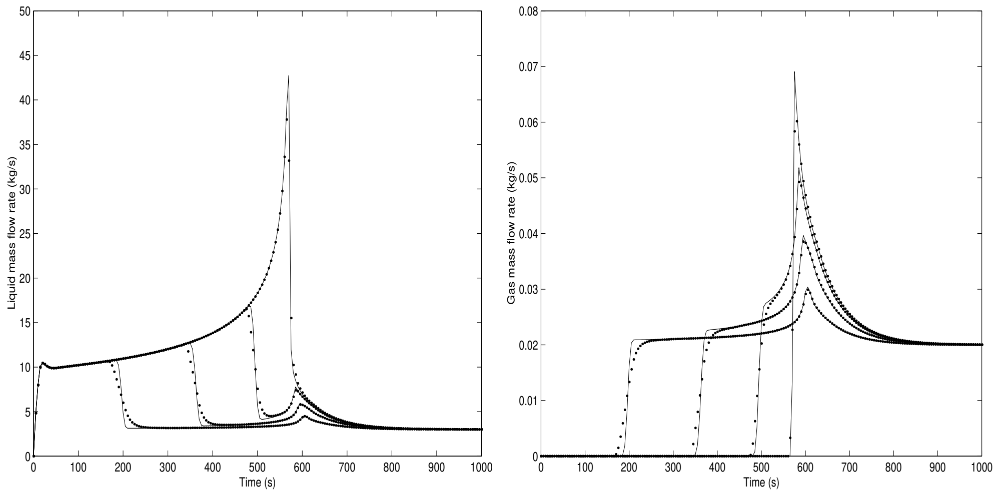

FIGURE 26. Primitive scheme. As in Fig. 23, liquid (left) and gas (right) flow rates are plotted at four different positions as functions of time.

the flow configuration; e.g., if gravitational forces are included in some parts of the flow region, the pressure gradient will increase and (22) will be easily (and unnecessarily) fulfilled if ε is not changed. Therefore it will be of importance to investigate other switching strategies that can be applied to compose efficient hybrid schemes. This will be the topic of future work.

Additional challenges that will be addressed in future work include (among others): (i) Extension of the hybrid schemes to models having variable geometry, which makes the flux functions highly (discontinuously) dependent on the space coordinate. (ii) Development of simple (partial) implicit strategies to even further speed up the hybrid schemes. The major limitation of explicit schemes is their stability constraint. This constraint imposes an upper limit on the allowed time step determined by the fastest (pressure) waves in the system. However, for the drift flux model the important physics occurs on time scales that are much longer than the scale associated with the pressure waves. In this case, the explicit schemes limit the time step to a much smaller value than is needed to accurately resolve the transient behaviour.

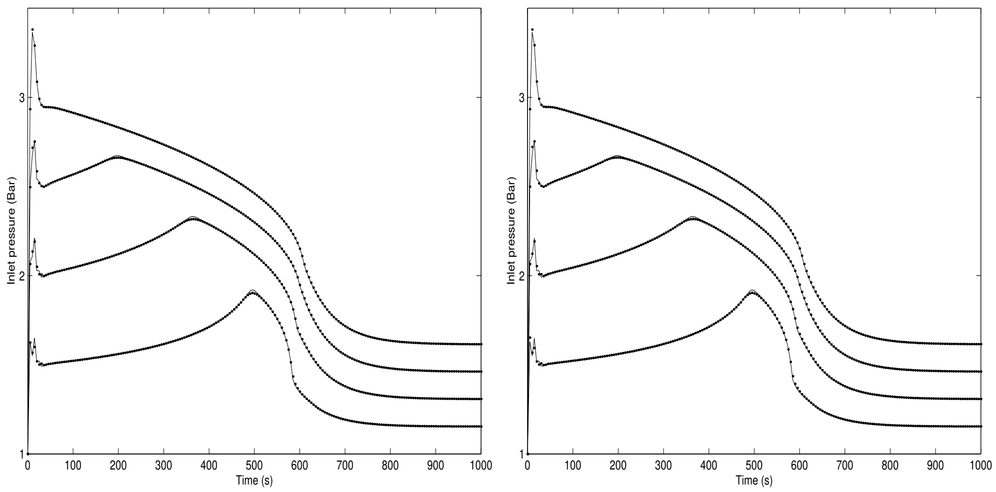

FIGURE 27. Pressure at positions $x = 0$ [m], 250 [m], 500 [m], 750 [m] as function of time. The upper curve corresponds to $x = 0$ [m] and the lowest to $x = 750$ [m]. Left: Roe scheme. Right: Rough Godunov scheme. The solid line represents the Reference solution.

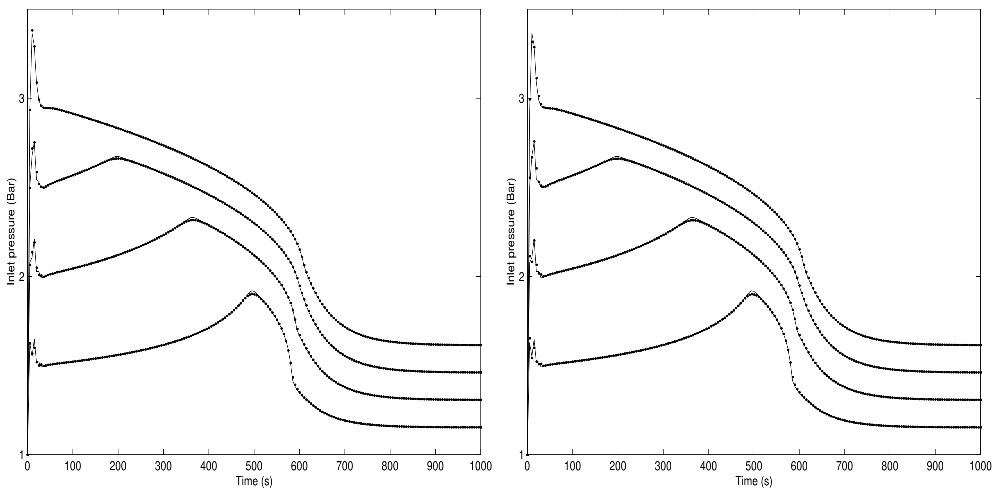

FIGURE 28. As in Fig. 27, pressure at four different positions as function of time. Left: Approximate-state Godunov scheme. Right: Primitive scheme.

REFERENCES

[1] K. Bendiksen, D. Malnes, R. Moe, and S. Nuland. The dynamic two-fluid model OLGA: Theory and application. *SPE Production Engineering*, pages 171–180, May 1991.

[2] S. Benzoni-Gavage. *Analyse numérique des modèles hydrodynamiques d'écoulements diphasiques instationnaires dans les réseaux de production pétrolière*. Thèse, ENS Lyon France, 1991.

[3] K. K. Fjelde and K. H. Karlsen. A comparative study of some fully numerical shock-capturing schemes for simulating two-phase flow. Preprint (in preparation).

[4] E. Harabetian and R. Pego. Nonconservative hybrid shock capturing schemes. *J. Comput. Phys.*, 105(1):1–13, 1993.

[5] T. Y. Hou and P. G. Le Floch. Why nonconservative schemes converge to wrong solutions: error analysis. *Math. Comp.*, 62(206):497–530, 1994.

[6] M. Ishii. *Thermo-Fluid Dynamic Theory of Two-Phase Flow*. Eyrolles, Paris, 1975.

[7] M. J. Ivings, D. M. Causon, and E. F. Toro. On hybrid high resolution upwind methods for multicomponent flows. *Z. Angew. Math. Mech.*, 77(9), 1997.

[8] S. Karni. Viscous shock profiles and primitive formulations. *SIAM J. Numer. Anal.*, 29(6):1592–1609, 1992.

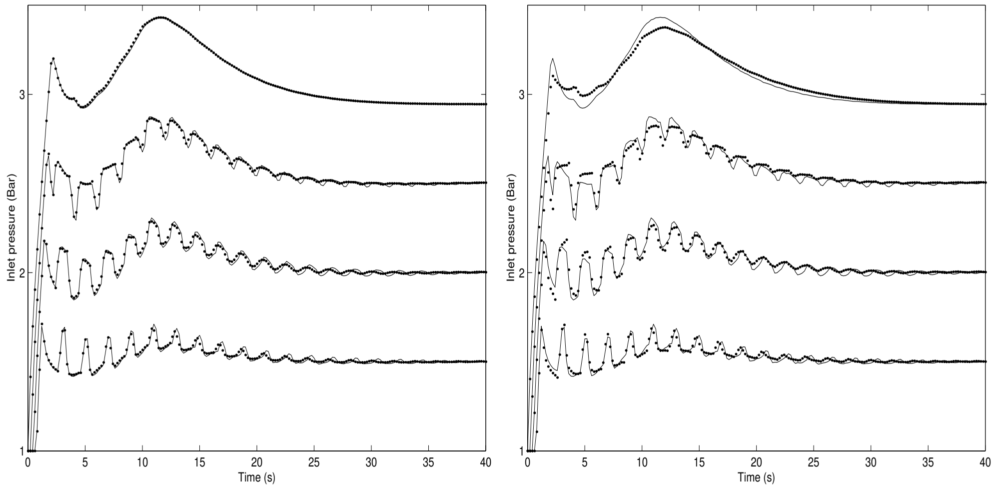

FIGURE 29. A closer look of the pressure behaviour in the early stage of the flow development. Left: Approximate-state Godunov scheme. Right: Primitive scheme. The solid line is the reference solution.

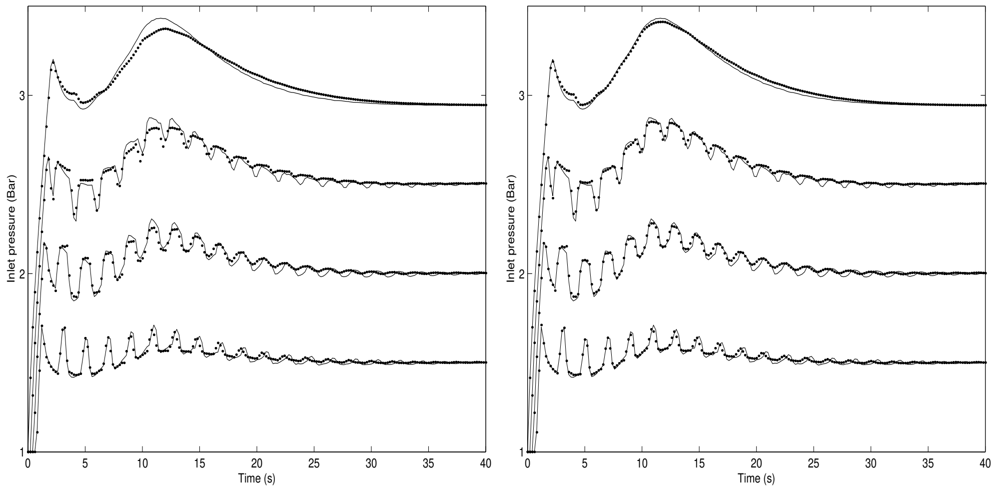

FIGURE 30. As in Fig. 29, a closer look at the pressure. Hybrid scheme based on the approximate-state Godunov scheme for the conservative updates. Left: Switch based on $\varepsilon = 0.01$. Right: Switch based on $\varepsilon = 0.0075$.

[9] S. Karni. Multicomponent flow calculations by a consistent primitive algorithm. *J. Comput. Phys.*, 112(1):31–43, 1994.

[10] S. Karni. Hybrid multifluid algorithms. *SIAM J. Sci. Comput.*, 17(5):1019–1039, 1996.

[11] R. J. LeVeque. *Numerical methods for conservation laws.* Birkhäuser Verlag, Basel, second edition, 1992.

[12] J. M. Masella, I. Faille, and T. Gallouet. On a rough godunov scheme. *Int. J. Computational Fluid Dynamics.* To appear.

[13] P. L. Roe. Approximate Riemann solvers, parameter vectors and difference schemes. *J. Comput. Phys.*, 43:357–372, 1981.

[14] J. E. Romate. An approximate Riemann solver for a two-phase flow model with numerically given slip relation. *Comput. & Fluids*, 27(4):455–477, 1998.

[15] B. Théron. *Ecoulements diphasique instationnaires en conduite horizontale.* Thèse, INP Toulouse, France, 1989.

[16] E. F. Toro. *Riemann solvers and numerical methods for fluid dynamics.* Springer-Verlag, Berlin, 1997. A practical introduction.

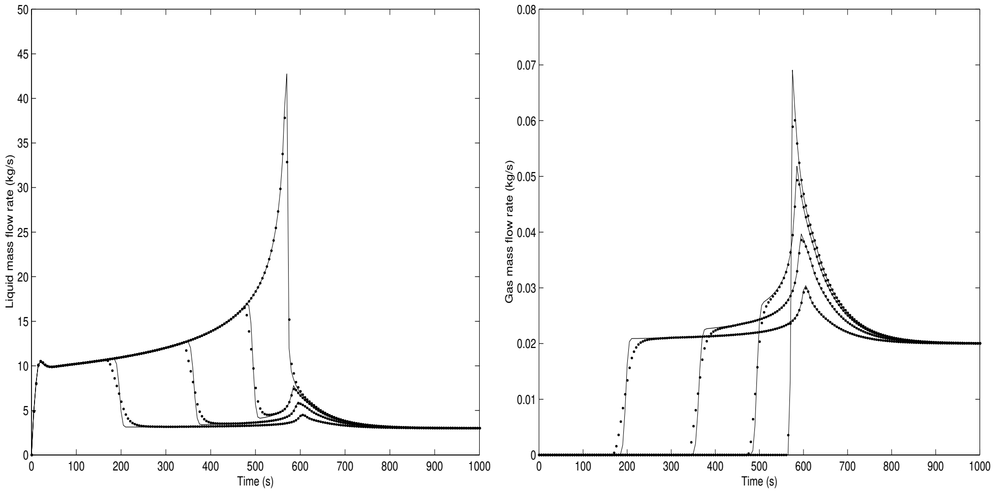

FIGURE 31. As in Fig. 23, mass flow rates predicted by a hybrid scheme (variable ε) based on the approximate-state Godunov scheme for the conservative updates.

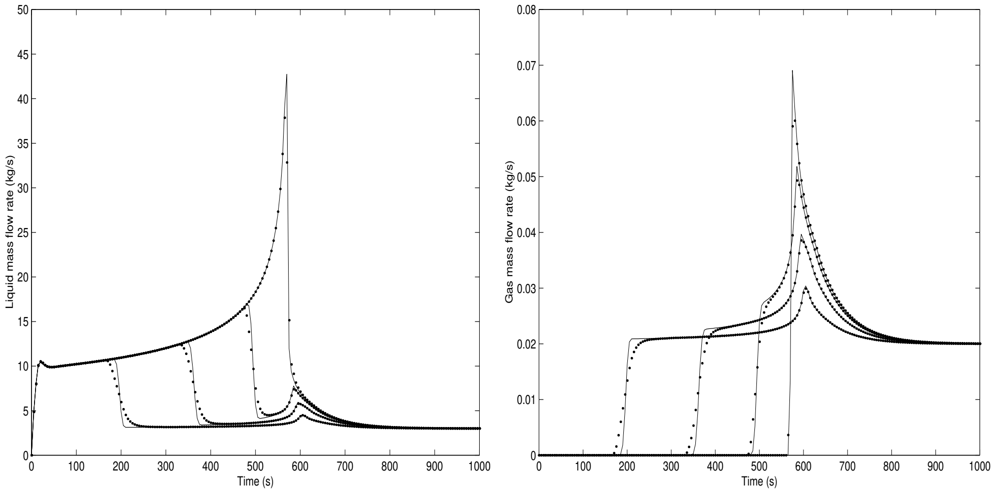

FIGURE 32. As in Fig. 23, mass flow rates predicted by a hybrid scheme (variable ε) based on the Roe scheme for the conservative updates.

[17] E. F. Toro. Primitive, conservative and adaptive schemes for hyperbolic conservation laws. In *Numerical methods for wave propagation (Manchester, 1995)*, pages 323–385. Kluwer Acad. Publ., Dordrecht, 1998.
[18] B. van Leer. Towards the ultimate conservative difference scheme. V. A second-order sequel to Godunov's method. *J. Comput. Phys.*, 32(1):101–136, 1979.
[19] B. van Leer. On the relation between the upwind-differencing schemes of Godunov, Engquist-Osher and Roe. *SIAM J. Sci. Statist. Comput.*, 5(1):1–20, 1984.

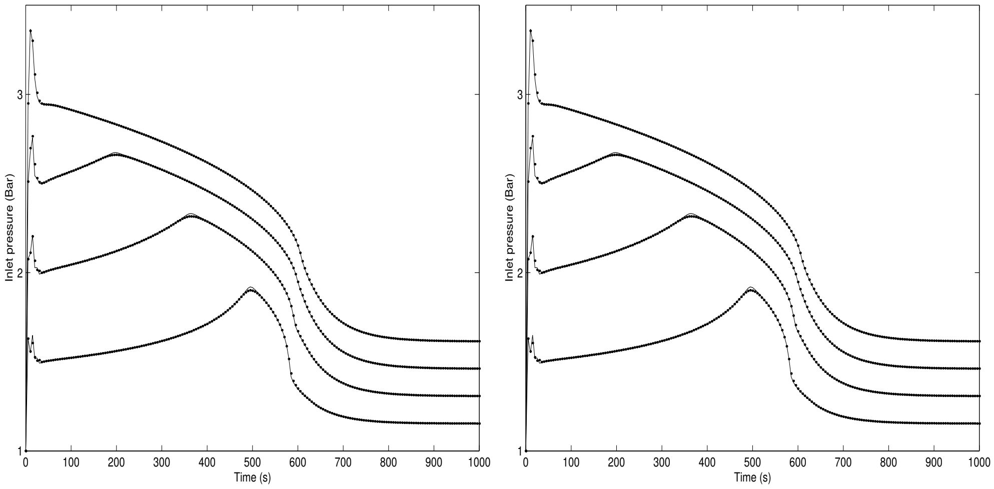

FIGURE 33. As in Fig. 27, pressure predictions. Left: Hybrid scheme (variable ε) based on the approximate-state Godunov scheme. Right: Hybrid scheme based on the Roe scheme.

CPU-time	
Roe scheme	1088.5 [s]
Rough Godunov scheme	1992.5 [s]
Approximate-state Godunov scheme	570.0 [s]
Primitive scheme	656.0 [s]
Hybrid-Roe scheme	670.6 [s]
Hybrid-approximate-state Godunov scheme	576.2 [s]

TABLE 1. Rough estimates of the CPU-time for the different schemes used in the example of transport of gas and liquid.